



저작자표시 2.0 대한민국

이용자는 아래의 조건을 따르는 경우에 한하여 자유롭게

- 이 저작물을 복제, 배포, 전송, 전시, 공연 및 방송할 수 있습니다.
- 이차적 저작물을 작성할 수 있습니다.
- 이 저작물을 영리 목적으로 이용할 수 있습니다.

다음과 같은 조건을 따라야 합니다:



저작자표시. 귀하는 원저작자를 표시하여야 합니다.

- 귀하는, 이 저작물의 재이용이나 배포의 경우, 이 저작물에 적용된 이용허락조건을 명확하게 나타내어야 합니다.
- 저작권자로부터 별도의 허가를 받으면 이러한 조건들은 적용되지 않습니다.

저작권법에 따른 이용자의 권리는 위의 내용에 의하여 영향을 받지 않습니다.

이것은 [이용허락규약\(Legal Code\)](#)을 이해하기 쉽게 요약한 것입니다.

[Disclaimer](#) 

Identification of DGAT2 as a key modulator
of mitochondrial dysfunction in
hepatocellular carcinoma

Yoseob Lee

Department of Medical Science
The Graduate School, Yonsei University

Identification of DGAT2 as a key modulator
of mitochondrial dysfunction in
hepatocellular carcinoma

Directed by Professor Sungsoon Fang

The Doctoral Dissertation
submitted to the Department of Medical Science,
the Graduate School of Yonsei University
in partial fulfillment of the requirements for the degree of
Doctor of Philosophy in Medical Science

Yoseob Lee

December 2023

This certifies that the Doctoral Dissertation of
Yoseob Lee is approved.

Thesis Supervisor : Sungsoon Fang

Thesis Committee Member#1 : Jae-woo Kim

Thesis Committee Member#2 : Kyung-Sup Kim

Thesis Committee Member#3: Heon Yung Gee

Thesis Committee Member#4: Seung Up Kim

The Graduate School
Yonsei University

December 2023

ACKNOWLEDGEMENTS

Throughout the long journey of integrative program that I had made in the graduate school, it is certain that none of my job is achieved by me alone. Thus, I would like to thank all the help and supports I have received.

First, I would like to call up my professor, Jae-woo Kim for all the teachings and trusts he gave to me. Without his supports, there is no way I would finish nor started my doctoral dissertation. Also, I could not hesitate to remark professor Sungsoon Fang. He is a trendsetter of our lab, to the new topics and new techniques. It is no doubt that my dissertation is full of his suggestions. I believe I was lucky enough to be taught by brilliant two professors, and it really broaden my perspective in research.

While spending most of daytime in the lab, it is a gift to meet colleagues know what I am doing. Mi-young Kim, Taehyun Kim and Bokyung Yoon are doctors in our lab. Their expertise and insights are the models to follow. Any new experiments and confusing data are solved with their experiences. Plus, I cannot miss my colleagues, Nahee Hwang, Kyu-Hye Chun, Jae-Won Kim and Hyeonuk Jeon. Their perspectives insight me in the field of biochemistry.

And it is always a great thank for Professor Kyung-Sup Kim, Heon Yung Gee, and Seung Up Kim to mentor my doctoral dissertation.

<TABLE OF CONTENTS>

ABSTRACT	i
I. INTRODUCTION	1
II. MATERIALS AND METHODS	4
1. RNA sequencing analysis	4
A. Data collection from different cohorts and projects	4
B. Transcriptome analysis	4
C. Drawing heatmap with transcriptome data	4
D. Kaplan-Meier survival plot	4
2. Lentivirus production and stable cell line transfection	4
3. Western blot assay	5
4. Cell culture	6
A. HepG2 cell culture	6
B. DGAT2 inhibitor treatment	6
5. Oxygen consumption rate analysis	6
6. Cell proliferation assay	6
7. Cell cycle assay	7
8. Wound healing assay	7
9. RNA extraction and Real-time quantitative PCR analysis	7
A. RNA isolation and cDNA synthesis	7
B. Quantitative PCR analysis	8
10. Preparation of nuclear and cytoplasmic fractions	8
11. Immunoprecipitation	8
12. Transmission electron microscopy	9
13. Integrated motif activity response analysis	10
14. ATAC sequencing	10
15. Confocal imaging of lipid droplet	10

16. TMRE assay: mitochondrial potential assay	10
17. mtDNA ratio assay	11
18. ATP assay kit	11
19. Lactate assay kit	11
20. Luciferase assay	12
21. Cholesterol assay kit	12
22. Spatial analysis	12
23. Statistical analysis	13
III. RESULTS	14
1. Construction and optimization of DGAT2 inhibitory cell model	14
2. Diminished mitochondria in DGAT2 KD HepG2 cell line	17
3. Mitochondrial dysfunction mediates impairments in energy production	20
4. Negative correlation of NAFLD and HCC patients	22
5. Lipid related genes can categorize HCC patients into severe and non-severe groups	25
6. DGAT2 expression follows patterns of lipid related DEGs	29
7. Low DGAT2 expression correlates with poor HCC outcomes	34
8. DGAT2 inhibition via chemical inhibitor and shRNA reveals increased cellular proliferation and migration in vitro	37
9. DGAT2 is more methylated in low DGAT2 expression group	41
10. ESRRA signal is downregulated when DGAT2 is inhibited	43
11. ESRRA-PROX1 transcriptional network is suppressing the ESRRA signal	46
12. Mitochondrial dysfunction is rescued with ESRRA overexpression	49
IV. DISCUSSION	54
V. CONCLUSION	57

REFERENCES	58
ABSTRACT(IN KOREAN)	63

LIST OF FIGURES

Figure 1. Construction and Optimization of DGAT2 inhibitory cell models	15
Figure 2. Regression of mitochondria in HepG2 cell line via DGAT2 knockdown	18
Figure 3. Loss of mitochondrial function upon DGAT2 inhibition	20
Figure 4. Correlation and differences in DEGs of NAFLD patients and HCC patients	23
Figure 5. Lipid metabolism is suppressed in HCC and indicates severity of patients	27
Figure 6. DGAT2 expression regresses in HCC patients	30
Figure 7. Correlation of DGAT2 expression level and clinical variances in HCC patients	32
Figure 8. Low DGAT2 expressing HCC are more severe than high DGAT2 expressing HCC	35
Figure 9. Metabolic differences in DGAT2 low HCC	36
Figure 10. Cell proliferation and migration is upregulated in DGAT2 inhibitory model	38
Figure 11. Glycolysis is upregulated in DGAT2 inhibitory model and promotes cell proliferation	40
Figure 12. Genomic analysis suggest methylation to be a regulator of DGAT2 expression	42
Figure 13. ESRRA motif, ERRE, is suppressed in DGAT2 KD model	

.....	44
Figure 14. ESRRA cofactors suppress ESRRA activity	47
Figure 15. Overexpression of ESRRA rescues mitochondrial function and cell proliferation	50
Figure 16. Mitophagy is promoted in DGAT2 KD model	52
Figure 17. Correlation of immune function with DGAT2 expression level.....	53

LIST OF TABLES

Table 1. 73 genes related with lipid metabolism	26
Table 2. List of patients from TCGA LIHC cohort with DGAT2 mutation	43

ABSTRACT

Identification of DGAT2 as a key modulator of mitochondrial dysfunction in hepatocellular carcinoma

Yoseob Lee

*Department of Medical Science
The Graduate School, Yonsei University*

(Directed by Professor Sungsoon Fang)

While the contribution of non-alcoholic fatty liver disease (NAFLD) on hepatocellular carcinoma (HCC) is keep increasing overtime, little is known how lipid metabolism plays its role in HCC. This article investigated the triacylglycerol (TG) synthesizing enzyme, diacylglycerol O-acyltransferase 2 (DGAT2) and the consequences of losing it in HCC. The role of DGAT2 in HCC is analyzed via loss-of-function assay. DGAT2 knockdown (KD) HepG2 cell line was analyzed via RNA sequencing and ATAC sequencing. These *in vitro* and bioinformatic data were further compared with different cohort of liver cancer patients and non-alcoholic fatty liver disease (NAFLD) patients to elucidate how DGAT2 is regulating cancer metabolism. Knockdown of DGAT2 in HepG2 cell line exhibits decrease in lipid accumulation, suggesting suppressed TG synthesis. Notable changes in HepG2 were a decrease in mitochondrial size and its function, calculated via oxygen consumption rate. In the aspect of the cancer cell line, DGAT2 KD HepG2 exhibits upregulated cell cycle, proliferation, and migration. Further analysis of transcriptome of NAFLD and HCC patients highlights negatively correlating

expression patterns in lipid-associated 73 genes. Cancer patients with the lower gene expression happen to face lower survival rate and this tendency is also applied with the expression of DGAT2. DGAT2 KD cell and liver patients' transcriptome show downregulation in transcription factor, estrogen related receptor alpha (ESRRA) via Integrated System for Motif Activity Response Analysis (ISMARA), correlates with ATAC sequencing data and luciferase assay. Overexpression of ESRRA in DGAT2 KD HepG2 rescued mitochondrial activity and size.

DGAT2 expression sustains the stability of mitochondria in hepatoma via downregulation of ESRRA-PROX1 transcriptional activity, ameliorates the cell proliferation in HCC.

Key words : hepatoma; NAFLD; mitochondria; diacylglycerol O-acyltransferase

Identification of DGAT2 as a key modulator of mitochondrial dysfunction in hepatocellular carcinoma

Yoseob Lee

*Department of Medical Science
The Graduate School, Yonsei University*

(Directed by Professor Sungsoon Fang)

I. INTRODUCTION

While viral hepatitis is well-known etiology of HCC, NAFLD is newly emerging and yet, confusing etiology for HCC patients¹. Viral hepatitis, HBV and HCV, are known as the major cause of liver cancer for accounting about 50% to 70% of HCC patients². However, the improvement of vaccine and treatments, the incidence and prevalence of viral infection are keep lowering. In contrast, the prevalence of NAFLD increased up to 25% globally in a decade^{3,4}. Consequently, the portion of NAFLD in HCC patients is robustly increased from 5% to maximum 30% in 2000 to 2020s respectively considering cryptogenic cirrhosis in HCC patients^{5,6}.

Chronic viral hepatitis develops cirrhosis and further advances into HCC. Nonetheless, viral hepatitis reverses with sufficient medication. However, unlike viral hepatitis, NAFLD has no specific medication approved by FDA, making it hard to ameliorate fatty liver progression into a cirrhosis⁷. Moreover, several cases had reported HCC progression directly from fatty liver or non-alcoholic steatohepatitis (NASH) without diagnosis of cirrhosis⁸. Due to high prevalence and

heterogeneity, NAFLD is more concerned as a key cause of HCC⁹. However, little is known about the role of lipid metabolism in HCC^{5,10}.

The term lipid metabolism comprises complex process including lipid uptake, de novo lipogenesis, lipid accumulation, lipolysis, β -oxidation and lipid secretion¹¹. Thus, it is important to know which portion of lipid metabolism is working in HCC¹². Most well-known usage of lipid in cancer cell is a source of energy, where fatty acids (FA) are utilized in β -oxidation to produce ATP. Apparently, upregulation of FA oxidation and de novo lipogenesis (DNL) is frequently detected in HCC. Moreover, accumulated lipids form lipid droplets in cells which relieves cell stress and enhances cell stability. Current issue in HCC lipid metabolism is DNL. For example, acetyl-CoA carboxylase 1 (ACC1), a first key enzyme of DNL, is reported to increase HCC cell survival in low glucose condition. Also, fatty acid synthase (FASN), a rate-limiting enzyme in DNL, is considered as a new therapeutic target of HCC. Down-regulation and inhibition of FASN in HCC are frequently reported to suppress HCC growth. In contrast, double knock out of ACC1 and ACC2, exhibited HCC-prone characteristics. In addition, ceramide metabolism, which found to be dysregulated in HCC, is counted as a new therapeutic target. Recent findings support that upregulation of ceramide synthesis helps patients' survival¹³. The role of lipid metabolism in HCC is heterogeneous and is not fully understood.

After its first discovery of new diacylglycerol acyltransferase 2 (DGAT2) in 2001, DGAT2 has been issued as a new therapeutic target of NAFLD^{14,15}. Multiple studies in rodents illustrates the potential therapeutic action of DGAT2 inhibition for fatty liver^{16,17}; moreover, the phase two clinical trial of DGAT2 inhibitor was performed in 2021. Thus, DGAT2 is primarily focused as a TG synthesizing enzyme and the other functions are underestimated¹⁸.

We focused on the correlation of DGAT2 enzyme and mitochondria in hepatocellular carcinoma. Mitochondrial dysfunction is known to be a hallmark of cancer. However, the incidence of how mitochondria is facing impairment are not fully understood. With its nature of sharing plasma membrane with endoplasmic reticulum, mitochondria are also considered as a hub for lipid synthesis such as phospholipid and even TG despite the well-known functions; a TCA cycle and β -oxidation. Thus, proteins located in mitochondrion is highly related to lipid metabolism. We analyzed the impact of DGAT2 KD on hepatoma cell line and evaluated the cell characteristics compared to those of HCC patients. In this article, we have shown the changes of lipid-related genes in NAFLD patients and HCC patients and the impact of DGAT2 knockdown on mitochondrion genes via downregulation of ESRRA transcription factor.

II. MATERIALS AND METHODS

1. RNA sequencing analysis

A. Data collection from different cohorts and projects

Overall transcriptome analyzed can be categorized into three group. First is a liver cancer patient cohort from the cancer genome atlas (TCGA) of national cancer institute. Second is two dataset produced from Jae-woo Kim's lab. And Last is cohorts from GEO database; GSE89632, GSE126848, GSE164359, GSE223201, GSE182593, GSE193084).

B. Transcriptome analysis

Analyses were mostly conducted in the R language environment and g:Profiler for gene ontology analysis¹⁹. Differentially expressed genes (DEGs) were processed using DESeq2²⁰ in between two groups with FDR cutoff of 0.25 and minimum fold change of 1.5. The DEGs obtained from DESeq2 is then processed to g:Profiler to find significantly enriched pathways based on the Molecular Signature Database (MSigDB; www.broadinstitute.org/msigdb).

C. Drawing heatmap with transcriptome data

Heatmap is drawn in R studio with package "pHeatmap". The pairwise correlation of each sample is calculated based on spearman correlation using normalized transcriptome data.

D. Kaplan-Meier survival plot

The survival plot of liver cancer patients are drawn using R studio and package "TCGAbiolinks". Clinical data including vital status, days to death, and days to last follow up are exported from clinical data embedded in TCGA database.

2. Lentivirus production and stable cell line transfection

Stable transfection of plasmid DNA is mediated via lentiviral system. First, lentivirus is produced via secondary generation packaging system, which includes transfer plasmids, pMD2.G envelope plasmid, and psPAX2 packaging plasmid. Plasmids were transfected via Lipofectamine2000 (ThermoFisher, Illinois, USA). 1×10^6 cells of HEK293T cell were plated on the day before transfection. On day 0, 2.5 μg of each plasmid was mixed with lipofectamine 2000 and transfected via manufacturer's protocol. Next day, change the media and incubate for 3 days. Then, the media is collected and centrifuged to remove cell debris. The supernatants, containing lentivirus, are aliquot and stored in deepfreezer.

3. Westernblot assay

Protein sample was extracted from cell line using whole cell lysis buffer (1% SDS in 60mM Tris-Cl). Then, the concentration of protein is measured with BCA Protein Assay Kit (ThermoScientific, IL, USA). Protein is, then, mixed with a laemmli sample buffer and boiled for 5 min. Protein samples were loaded to the SDS-PAGE and then transfer to the Polyvinylidene fluoride (PVDF) membrane (Millipore, MA, USA). The membrane was blocked with 5% skim milk and primary antibody was applied as manufacturer's protocol. Horseradish peroxidase attached secondary antibody was treated according to the host of a primary antibody. The expression level of target proteins were detected with ECL. Antibodies used in westernblot experiments are correspond to the following lists. α -tubulin (Santa Cruz, TX, USA), B-actin (CST, MA, USA), Calnexin (Millipore, MA, USA), CCNA2 (Santa Cruz, TX, USA), CCNB1 (Santa Cruz, TX, USA), CCNE1 (Santa Cruz, TX, USA), CDK2 (BD, NJ, USA), COX4 (Santa Cruz, TX, USA), DGAT2 (Invitrogen, MA, USA), ESRRA (CST, MA, USA), Lamin A/C (Santa Cruz, TX, USA), LAMP1 (Santa Cruz, TX, USA), LC3B (CST, MA, USA),

PGC1A (Abcam, Cambridge, UK), and PROX1 (Biolegend, CA, USA).

4. Cell culture

A. HepG2 cell culture

HepG2 cell line is cultured in Dulbecco's modified eagle's media (DMEM) containing high glucose, glutamine, and sodium pyruvate (Gibco) supplied with 10 % FBS(Gibco) and 1% phenylsiline and streptomycin solution . Media is changed for every three days. When reaches 80-90 % confluency, HepG2 is split into 5 cell plates. All experiments were performed within 10 passages.

B. DGAT2 inhibitor treatment

DGAT2 inhibitor is constructed from pfizer (PF-06424439), which has IC₅₀ of 14 nM. 1 μ M of inhibitor is treated for 48 hrs.

5. Oxygen consumption rate analysis

oxygen consumption rate is measured with seahorse XFe96 mitochondria stress test kit. The assay is performed based on the manufacturer's protocol. Briefly, HepG2 cells were plated in 8,000 cells/well a day before the assay. Oligomycin, FCCP, and rotenone and antimycin are treated with the final concentration of 2.5 μ M, 1 μ M, and 2.5 μ M each respectively. After the assay, the OCR data is normalized according to the protein concentration.

6. Cell proliferation assay

Cell proliferation rate is calculated via CCK-8 reagent, which measuring the dehydrogenase activity of cells. 5,000 cells were plated on 96 well and incubated for 12 hrs for cell attachment. Then, 10 μ l of CCK-8 reagents were added to the cells and incubated for 1 hr. The amount of reaction is calculated with colorimeter

in 450 nm.

7. Cell cycle assay

Cell cycle is performed to compare the ratio of cells in specific phases via DNA staining using propidium iodide. 1×10^6 cells were plated on 60mm dish. When cell is stabilized, it is incubated in serum free media for 8 hrs to synchronize cell cycle phase. Then, the media is substituted to normal and incubated for 24 hrs. The cells are detached using trypsin-EDTA solution and then rinsed with PBS. Fixed with 100 % ethanol. PI is treated with RNase for DNA staining and PI is measured with SA3800.

8. Wound healing assay

1×10^6 cells were plated on 35mm cell plate dish. When reaches 100% confluency, cell is wounded using a white tip. The scar is pictured with bright field microscopy every day to track wound closure. Microscopy picture is analyzed with ImageJ software.

9. RNA extraction and quantitative PCR analysis

A. RNA isolation and cDNA synthesis

RNA is isolated from cell using TRIzol reagent (Invitrogen, MA, USA) with manufacturer's protocol. Briefly, after media removal, cell is lysed with TRIzol. 1-Bromo-3-chloropropane (BCP) is mixed and incubated for 10 mins in RT. Then 10,000 xg centrifugation for 15 mins for phase differentiation. The upper clear supernatants, composing RNA, is carefully moved to 1.5 ml microcentrifuge tube and 1ml of 100% isopropanol (Merck) is added to precipitate RNA after centrifugation for 10 mins. RNA is then pelleted and

washed with 70 % ethanol with DEPC treated water for twice. Pellet is now rinsed and resuspended in DEPC treated water. Which is processed into reverse transcription with SuperScript reverse transcriptase III (Invitrogen, MA, USA) and random hexamer.

B. Quantitative PCR analysis

cDNA is further analyzed with quantitative PCR. SYBR Green PCR Master Mix (Applied Biosystems, MA, USA) is used to detect DNA synthesis and $\Delta\Delta$ -Ct method was used to quantify the original DNA level. Data were normalized with 18S ribosomal RNA expression level. The primers used for qPCR is DGAT2-S: 5'-GAA TGG GAG TGG CAA TGC TAT-3'; DGAT2-AS: 5'-CCT CGA AGA TCA CCT GCT TG-3'; 18S-S: 5'-CTA CCA CAT CCA AGG AAG GCA-3'; 18S-AS: 5'-TTT TTC GTC ACT ACC TCC CC-3'.

10. Preparation of subcellular fractions

The subcellular fraction of cell was performed via different centrifugal forces. Cell was scraped from 100 mm cell culture plate with 500 μ l of fractionation buffer. Fractionation buffer is made of 20 mM HEPES, 10 mM KCl, 2mM MgCl₂, 1 mM of EDTA and 1 mM of EGTA. The cell is lysed by passing through 27G needle for 10 times. The suspension is then incubated on ice for 20 mins. Centrifuge the suspension with 720 xg for 5 mins to obtain pellets enriched with nucleus fraction and supernatants enriched with other organelles. The pellet is washed with fractionation buffer and resuspended with TBS containing 0.1 % SDS. The supernatant is centrifuged with 10,000 xg for 5 mins. This pellet is a fraction enriched with mitochondria. The supernatant is now composed of cytosol and ER fractions.

11. Immunoprecipitation

Cell, cultured on 100mm culture dish, is washed with PBS and scraped in 1ml of PBS. The cell suspension is centrifuged with 300 xg for 3 mins to collect pellets only. Add 500 μ l of lysis buffer and vortex for 5 mins. After the vortexing, cell lysate is centrifuged for 15,000 xg for 10 mins to remove cell debris. The supernatants are performed BCA assay to find the concentration of proteins. 500 μ g of proteins are transferred to new microcentrifuge tube with 20 μ l of protein A/G plus agarose (Santa Cruz, TX, USA). The sample is rotated in 20 rpm in the cold room for 2 hrs to remove unspecific bindings with A/G beads. 1 μ g of the target-specific antibody is added to cleaned sup and incubated with 20 rpm rotation in the cold room for 12 hrs. After the antibody binding, 40 μ l of protein A/G plus agarose are added and again rotated for 2 hrs. The beads are ;then, pulled down with 5,000 rpm centrifuge for 1 min and washed. 2x laemmli's buffer is added to the bead and boiled to detach the proteins. The recipe for lysis buffer is 50mM Tris-Cl, 0.3% NP-40, 0.2% Triton X-100, 150mM NaCl, 1mM Na₃VO₄ and protease inhibitor cocktail.

12. Transmission electron microscopy

Cell was rinsed with PBS and detached using Trypsin-EDTA (ThermoFisher, MA, USA). The cell is pelleted with 200 rpm centrifugation and fixed with 2.5% glutaraldehyde for overnight. The fixed sample is embedded with Poly/Bed 812 kit (Polysciences), polymerized in an electron microscope oven(TD-700, DOSAKA, Japan) at 65 $^{\circ}$ C for 12 hrs. Sample block is cut into 200nm semi-thin section and stained with toluidine blue, and section again into 80nm thin layer and placed on a copper grid. The final sample is observed with TEM (Jeol, Tokyo, Japan).

13. Integrated motif activity response analysis

Integrated Motif Activity Response Analysis (ISMARA) is a web-based tool to predict the activity of regulatory DNA motifs using the transcriptome data and the motifs within the promoters of each gene. For process, .fastq file data were compared with hg38 genomics references.

14. ATAC sequencing

Raw fastq files are processed quality check and trimming with Trim Galore. The reads are aligned and paired with Bowtie2, samtools, Picard and shell script. MACS2 and Chipseeker packages are used for peak calling and annotation. The following processes are performed via MACROGEN.

15. Confocal imaging of lipid droplet

14 to 18pi cover glasses are washed with 1N NaOH solution, rotated in cold room for overnight. Then, cover glasses are rinsed with distilled water for three times. A single cover glass is placed on 12 well plate and 0.01% collagen type I (Sigma-Aldrich, MO, USA) is applied on the cover glass. 2.5×10^5 cells are plated and incubated 4-12 hours for attachments. Cells are treated with 200 mM oleic acid and 200 mM palmitic acid for 4 hours with or without 1 μ M of DGAT2 inhibitor. Then, the samples are washed and fixed with neutral formalin for 5 minutes. Fixed samples are rinsed and performed staining process via BODIPY and DAPI. Stained samples are mounted on slide glass using mounting medium, The final samples are detected with LSM700 microscopy.

16. TMRE assay: mitochondrial potential assay

HepG2 cell lines (HepG2 shCTR and shDGAT2) are subcultured on black 96 well plate, 1.0×10^5 cell/well. On the next day, half of the wells are treated with 20 μ M FCCP for 10 minutes to remove mitochondrial potential. Then, 250 nM tetramethylrhodamine, ethyl ester (TMRE) are treated on the plate for 30 minutes. The TMRE solution is rinsed with 0.2% BSA-PBS solution for twice and the fluorescence level are measured with fluorometer Varioskan Flash 3001 (Thermofisher scientific).

17. mtDNA ratio assay

Genomic DNA is extracted from cell line via genomic DNA extraction kit (BIONEER, Daejeon, Korea). gDNA is performed quantitative PCR to calculate ratio of mtDNA and reference gene, mt-ND1 and pyruvate kinase (PK). Primers used are mt-ND1 F: 5'-CCCTAAAACCCGCCACATCT-3' and R: 5'-GGCCTA GGTGAGGTTGACC-3'; PK F: 5'-ATAACGCCTACATGGAAAAGTGT -3' and R: 5'-TAAGCCCATCATCCACGTAGA-3'.

18. ATP assay kit

Cellular ATP level is measured with ATP assay kit (Abcam, Cambridge, UK) following the manufacturer's protocol. Briefly, cell is homogenized in ATP assay buffer and supernatants are collected after centrifugation. Samples and ATP standards are incubated with reaction mixture for 30 minutes. The reaction products are measured via colorimeter (OD570 nm) via Multiskan GO (Sigma-Aldrich, MO, USA).

19. Lactate assay kit

Cellular lactate level is measured with EZ-Lactate Assay kit (DoGenBio, Seoul,

Korea). Cell lysate is prepared with 2×10^6 cells homogenized in assay buffer. Supernatants are collected from centrifuged sample. 50 μ l of samples and lactate standards are incubated with enzyme mixture for 30 minutes in RT and measured colorimetric absorbance on A570 with Multiskan GO.

20. Luciferase assay

p3xERRE-firefly luciferase plasmid (Addgene, MA, USA) and renilla luciferase plasmids are transfected to HepG2 cell line via lipofectamine 3000. After a day passed, dual-luciferase reporter assay system (Progenia, WI, USA) is used to calculate activity of luciferases translated according to manufacturer's protocol. Briefly, cell lysate is prepared with passive lysis buffer. Then using Centro XS3 LB960 luminometer (EG & G Berthold) to add luciferin and stop solution to detect the activity of firefly luciferase and renilla luciferase separately for normalization.

21. Cholesterol assay kit

Cellular total cholesterol levels are measured with cholesterol assay kit (Abcam, Cambridge, UK). Cellular lysates of lipids are prepared via Folch extraction. The experiments are performed as manufacturer's protocol. Briefly, Folch extracted samples and cholesterol standards are added to 96 well plate and added with master reaction solution; then, the reaction is held in 37 °C, light protected for 1 hour. The final product is measured in colorimeter with OD570 nm.

22. Spatial analysis

Spatial dataset was available from GSE192741 (healthy = 2, steatosis =3) and from supplementary data of DOI: 10.1126/sciadv.abg3750 (normal = 4, tumor = 4). The dataset was analyzed with R version 4.3.1 and Seurat_4.4.0 package

following the ‘Analysis of Image-based Spatial Data in Seurat’ from satijalab. Briefly, dataset and high-resolution image files were loaded to R and normalized with `sctransform_0.4.1`. Normalized data were integrated and performed standard workflow of single cell RNA sequencings; `ScaleData`, `RunPCA`, `RunUMAP`. `Sctransform` normalized data was presented via `VlnPlot` and `SpatialFeaturePlot`.

23. Statistical analysis

All statistical analyses were performed under consideration of the experimental method and characteristics of data. If the data fits in normal distribution, parametric methods are used and if not, non-parametric methods are used. Normality test is performed with Shapiro’s test. For parametric test, student’s t-test is used. For non-parametric test, mostly Mann Whitney U-test is utilized for calculating significance of correlation between two factors. Also, spearman correlation, long rank test, one-way ANOVA and False discovery rate (FDR) is used for specific methods and are mentioned in the figure legends. The p-values under 0.05 was considered as statistically significant value. * p-value < 0.05, ** p-value < 0.01, *** p-value < 0.001, **** p-value < 0.0001. All data are shown with mean and standard deviation, unless specified.

III. RESULTS

1. Construction and optimization of DGAT2 inhibitory cell model

DGAT is a major TG synthesis enzyme in mammalian cell and considered as a promising therapeutic target of obesity and NAFLD. To understand metabolic role of DGAT2 in liver, I inhibited either activity or expression of DGAT2 from HepG2 cell line to perform loss-of-function assay (Fig. 1A). For activity inhibition, DGAT2 specific inhibitor (PF-06424439) is used and was able to find out that 1 μ M of concentration is sufficient to inhibit lipid droplet (LD) formation with 400 mM of oleic and palmitic acid treatment (Fig. 1B-1C). To suppress *DGAT2* expression, shRNA was transfected via lentivirus. Three different shRNA sequences were tested and TRCN0000005196 shRNA suppressed about 80% of DGAT2 expression permanently in HepG2 cell line (Fig. 1D). With the loss of mRNA, protein level of DGAT2 decreased from DGAT2 KD model (Fig 1E). Altogether, inhibitor treatment and shRNA transfection suppressed LD formation in cell under fatty acid administration (Fig. 1F-1G). The following models were used for *in vitro* models to observe role of DGAT2.

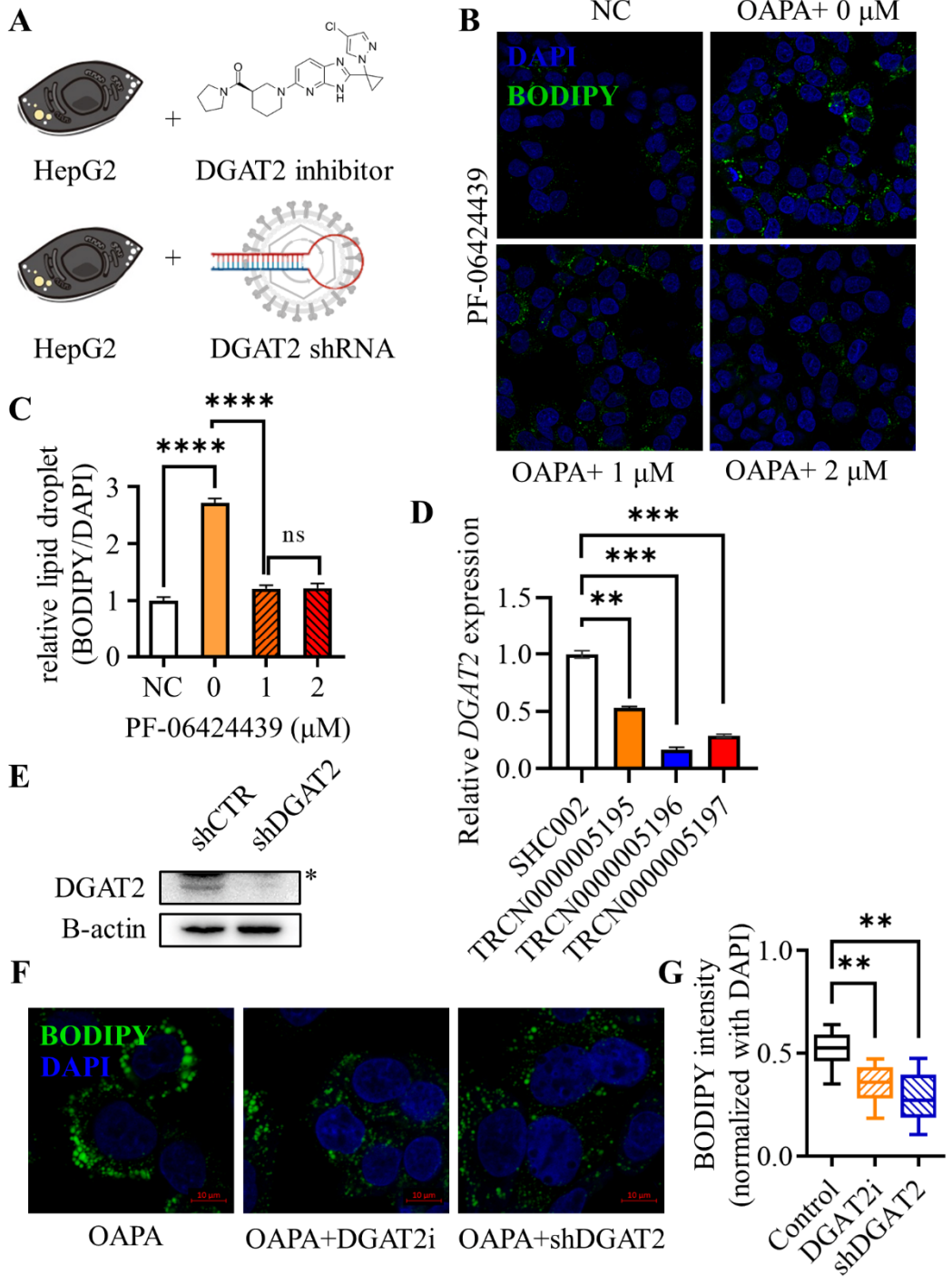


Figure 1. Construction and Optimization of DGAT2 inhibitory cell models. (A) Schematic illustration explaining the treatment used for DGAT2 inhibition. First model uses DGAT2 specific inhibitor to block DGAT2 activity and second model uses *DGAT2* shRNA to suppress expression. (B) Confocal images show inhibition of lipid droplet (LD) formation upon serial DGAT2 inhibitor treatments. NC is a negative control without oleic acid and palmitic acid treatment whereas OAPA + 0 μ M is a group with fatty acid treated 200 mM each. (C) The intensity of BODIPY is measured relative to intensity of DAPI, which exhibits significant decrease of LD upon inhibitor treatment. (D) Relative expression level of *DGAT2* suggests TRCN0000005196 to be a most efficient shRNA for DGAT2. (E) Suppressed DGAT2 protein level via shRNA treatment. Asterisk is to indicate unspecific band. (F) Confocal image of LD from the stabilized DGAT2 inhibitory model. (G) DGAT2 activity is inferred from LD formation. The relative intensity is calculated. Data represent mean + SD. ** $p < 0.01$, *** $p < 0.001$, **** $p < 0.0001$; student's t-test, two tailed.

2. Diminished mitochondria in DGAT2 KD HepG2 cell line

The location of DGAT2 is known as an ER and it is discovered that ER and mitochondria shares their membrane in between a short gap of 20-40nm distance. This portion of membrane is called as mitochondria-associated membrane (MAM) and known to be a hub of lipid synthesis^{21,22}. However, it is not considered how DGAT2 would modify mitochondria. Therefore, diminished mitochondria was unexpected changes from DGAT2 KD HepG2 cell. Transmission electron microscopy (TEM) images were taken from both control and DGAT2 KD samples and the portion of mitochondria, dark gray organelle, was reduced in DGAT2 KD sample (Fig. 2A). Moreover, confocal image of mitochondria exhibits droplet like structure in DGAT2 KD, while looked linear in control sample (Fig. 2B). These observation is quantified with ImageJ and found that mitochondrial area and lengths are significantly decreased in DGAT2 KD sample (Fig. 2C-2D). Due to significant differences in mitochondrial morphology, the aspects of mitochondria were assessed. Normally, mitochondria with high membrane potential in intermembrane is healthy. TMRE stains mitochondria according to proton gradient and DGAT2 KD sample shows more than 10-fold differences with control (Fig. 2E). Moreover, mtDNA ratio is decreased in DGAT2 KD HepG2, which indicates impairment of mitochondria (Fig. 2F). There would be several possibilities for the impairment; however, since mitochondria is a dynamic organelle, I focused on fission and fusion of mitochondria in DGAT2 KD cell and observed upregulation of fission promoting mitochondrial fission 1 (FIS1) and dependent mitochondrial fission (DRP1) with serine 616 phosphorylation, while fusion promoting serine 637 phosphorylation of DRP1 is not detected (Fig. 2G). Thus, DGAT2 KD HepG2 faces mitochondrial dysfunction.

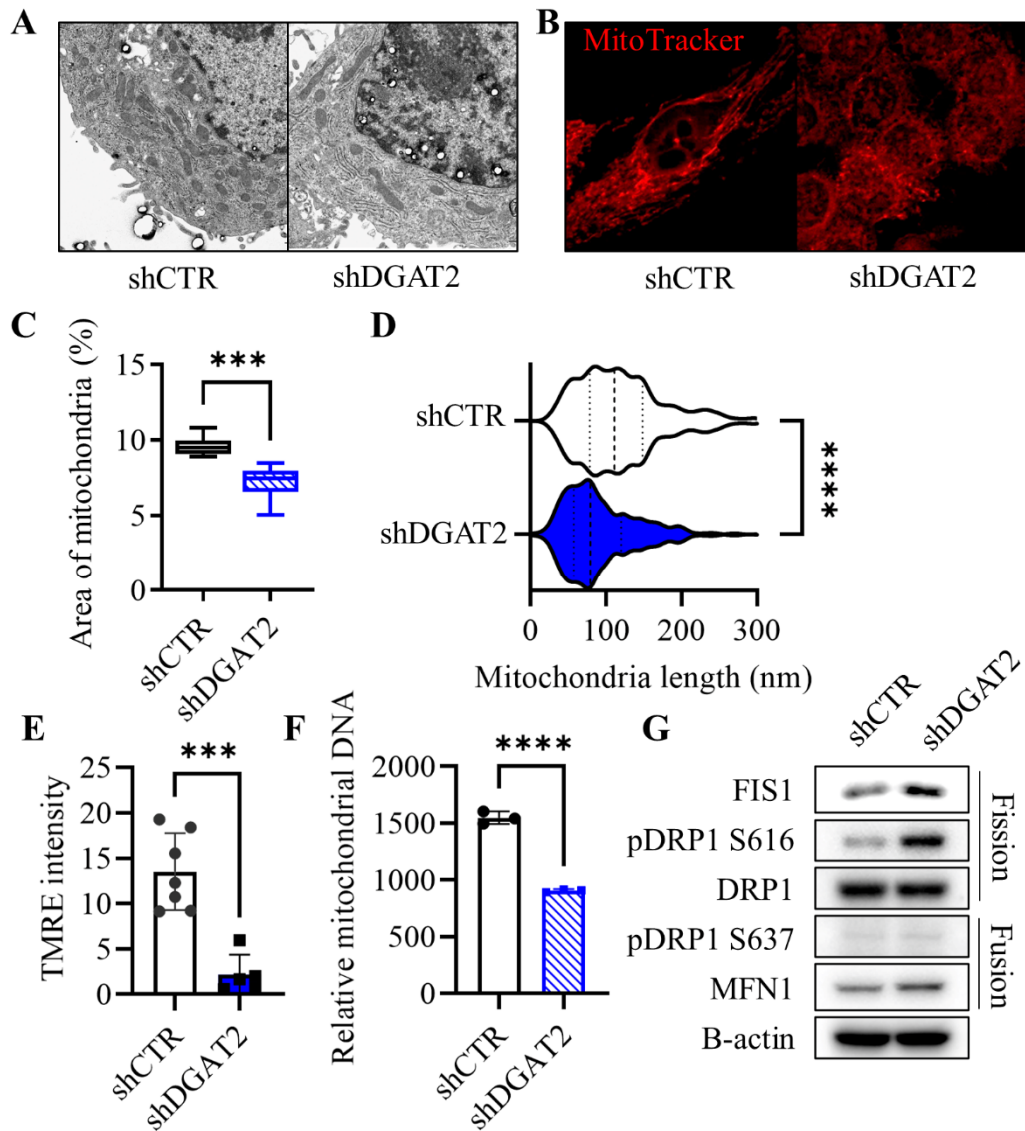


Figure 2. Regression of mitochondria in HepG2 cell line via *DGAT2* knockdown. (A) TEM image of HepG2 *DGAT2* KD model. dark gray organelle in cytosol area indicates mitochondria. the density of mitochondria is diminished in sh*DGAT2* model. (B) Confocal image of HepG2 *DGAT2* KD model. Mitochondria is stained in red with MitoTracker DeepRed. Morphologies of mitochondria is circular in sh*DGAT2* model. (C) Area of mitochondria is measured from random 20 TEM images with ImageJ. Mitochondrial area

relative to cytosol area suggests significant decrease of mitochondria in shDGAT2 model. (D) Mitochondrial lengths are measured with ImageJ from 20 random TEM images. The distribution of mitochondrial length was shortened in shDGAT2 model. (E) Membrane potential of mitochondria is measured with TMRE staining, which decreased in DGAT2 KD model. (F) The proportion of mtDNA to genomic. (G) Fission and fusion proteins were detected. Proteins inducing fissions, FIS1 and pDRP1 S616, are upregulated in DGAT2 KD model. Data represent mean +SEM for (C) and (D) and mean + SD for (E). *** $p < 0.001$, **** $p < 0.0001$; student's t-test, two tailed.

3. Mitochondrial dysfunction mediates impairments in energy production

As an energy factory, mitochondria convert acetyl-CoA to ATP. Thus, DGAT2 inhibition decreases oxygen consumption rate (OCR). Moreover, DGAT2 KD HepG2 cell utilizes less fatty acid as a fuel that CPT1 inhibition via etomoxir treatment does not exhibit OCR differences in DGAT2 KD sample, while OCR level decreased in control sample (Fig. 3B). As consequence, cellular level of ATP from DGAT2 inhibitory models were lower than that of control sample (Fig. 3C).

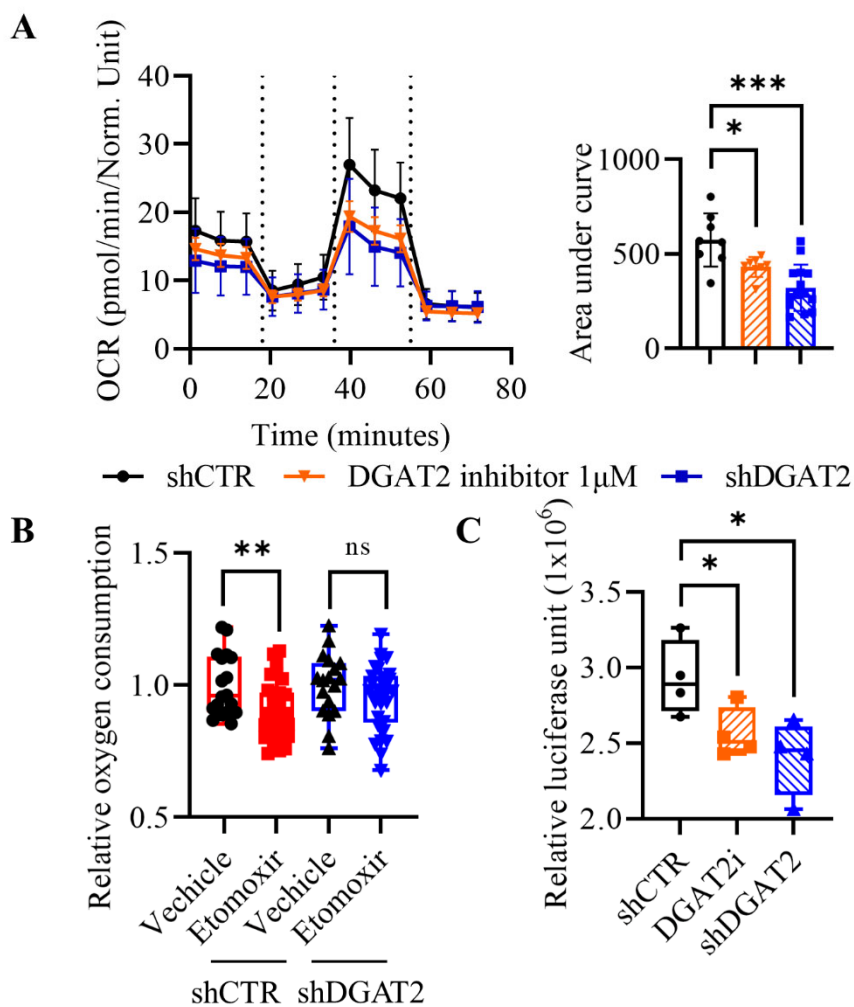


Figure 3. Loss of mitochondrial function upon DGAT2 inhibition. (A) Oxygen consumption rate is measured for mitochondrial activity. Inhibition of DGAT2 lowers maximal respiratory capacity, which is measured via area under curve and plotted on right. (B) Inhibition of fatty acid transport via CPT1 inhibitor, etomoxir, does not changed oxygen consumption in DGAT KD model. (C) Cellular ATP level is measured from DGAT2 inhibitory cell lines. Data represent mean + SD. * $p < 0.05$, ** $p < 0.01$, *** $p < 0.001$; student's t-test, two tailed.

4. Negative correlation of NAFLD and HCC patients

Assume the liver disease as a progression toward HCC, NAFLD is now a major etiology for HCC development. Inhibition of DGAT2 is still considered to be a therapeutic method for NAFLD treatment, and loss of mitochondrial function is considered as a cancer hallmark. To further understand correlation of NAFLD and HCC, cumulative analysis of transcriptomic data of NAFLD patients and HCC patients were performed to identify differentially expressed genes (DEGs) (Fig. 4A). Comparing other sections of Venn-diagram, 2,148 upregulated genes in both NAFLD and HCC patients. 617 DEGs were downregulated in NAFLD but upregulated in HCC. 805 genes were, in contrast, upregulated in NAFLD but downregulated in HCC. 1,414 genes were downregulated both groups. Analyzing via g:Profiler²³, each group is composed with important pathways in terms of NAFLD and HCC. DNA replication and cell cycle is upregulated in both diseases (Fig. 4B). 1,414 genes are related in protein synthesis and cell integrity (Fig. 4C). 804 genes are composed with metabolic genes, especially lipid related pathways (Fig. 4D), and 617 genes suggest various signaling are downregulated in both diseases (Fig. 4E).

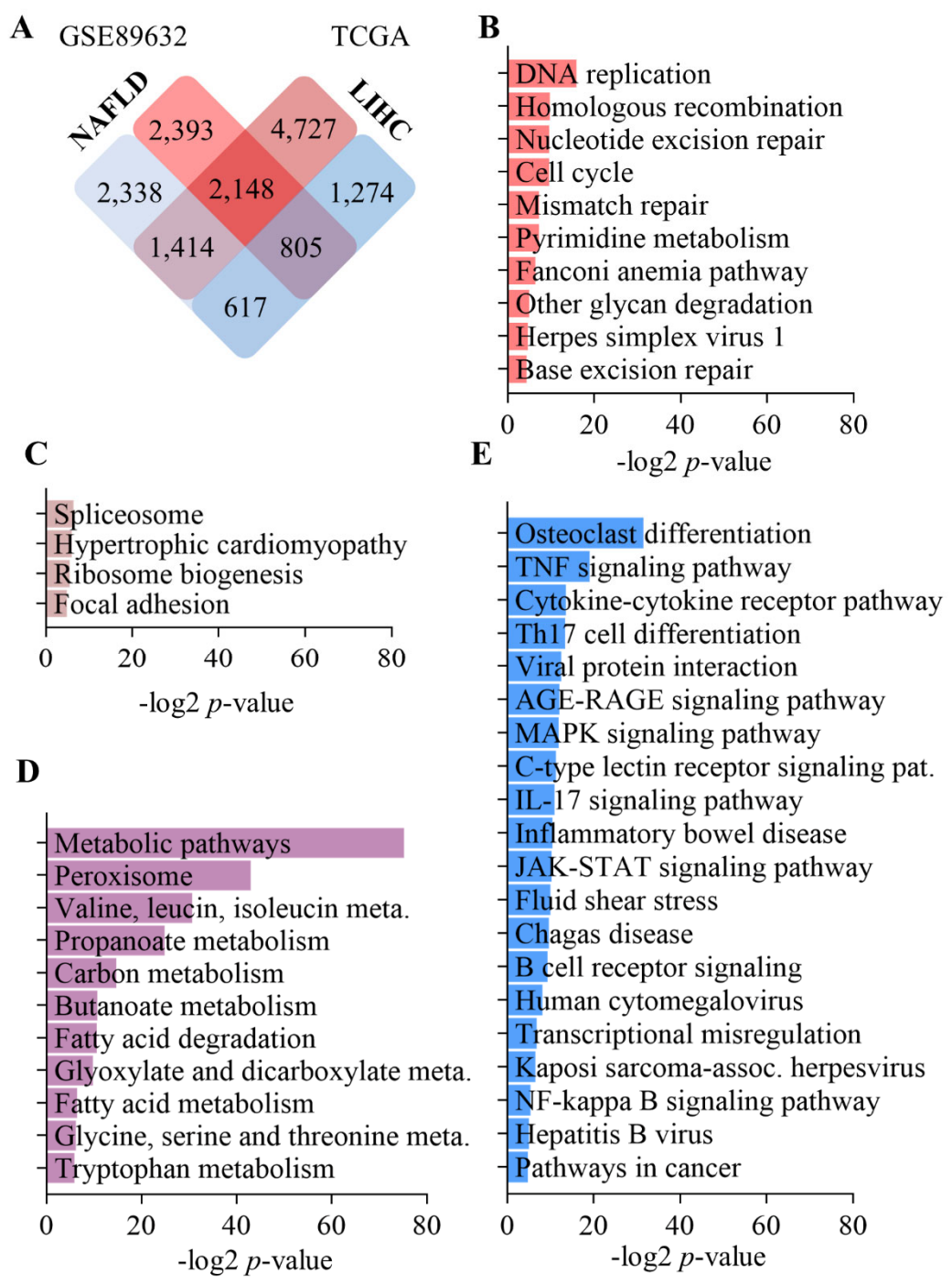


Figure 4. Correlation and differences in DEGs of NAFLD patients and HCC patients.

(A) Venn diagram of DEGs from NAFLD patients (GSE89632; healthy = 24, NAFLD = 39) and HCC patients (TCGA-LIHC; Adjacent tissue = 50, HCC = 371). (B-E) Enriched KEGG pathways from (B) 2,148 DEGs both upregulated from NAFLD and HCC patients. (C) 1,414 DEGs downregulated in NAFLD patients while upregulated in HCC patients. (D) 805 DEGs upregulated in NAFLD patients while downregulated in HCC patients. (E) 617 DEGs both downregulated in NAFLD and HCC patients. DEGs are processed via DESeq2 packages. The significance is calculated with false discovery rate.

5. Lipid related genes can categorize HCC patients into severe and non-severe groups

805 DEGs, which are upregulated in NAFLD patients while downregulated in those of HCC, are related with lipid metabolism, which were not observed in other groups. Of 805 genes, 73 genes directly participate in lipid metabolism according to the Kyoto encyclopedia of genes and genomes (KEGG) (Fig. 5A, Table 1). Markedly, 73 genes categorize HCC patients into three different groups: group 1, group 2, and group 3 (Fig. 5B). According to the PCA, group 1 and group 3 are clustered with each other, while group 2 is placed in between two groups (Fig 5C). Patients with higher 73 gene expression such as group 1 tends live longer (p -value=0.018) than those of whom exhibit lower gene expression (Fig. 5D).

Table 1. 73 genes related with lipid metabolism

Genes					
ACAA1	ADH4	CYP39A1	MOGAT2	PIK3C2G	SMPD3
ACACB	ADH6	CYP4F2	MTM1	PIK3R1	SPHK2
ACADL	AGPAT2	DGAT2	MVK	PLA2G12A	SPTLC3
ACADS	AKR1D1	ELOVL6	NR1H3	PLD1	SRD5A2
ACAT1	ALDH1B1	EPHX2	NUDT7	PLIN1	STARD5
ACBD4	APOA5	GPD1	ORMDL3	PNPLA3	THRSP
ACBD5	BDH1	HADH	PCCB	PON1	TNFAIP8L1
ACOT12	CBR4	HAO2	PCTP	PRKAG2	TNFAIP8L2
ACOT2	CEPT1	HMGCL	PECR	PTGS1	
ACOT4	CPT2	HSD17B8	PEMT	SEC24B	
ACOX1	CRAT	MCAT	PEX11A	SLC10A1	
ACOX2	CYP27A1	MCEE	PHYH	SLC25A20	
ACSM3	CYP2U1	MGLL	PI4K2B	SLCO1B1	

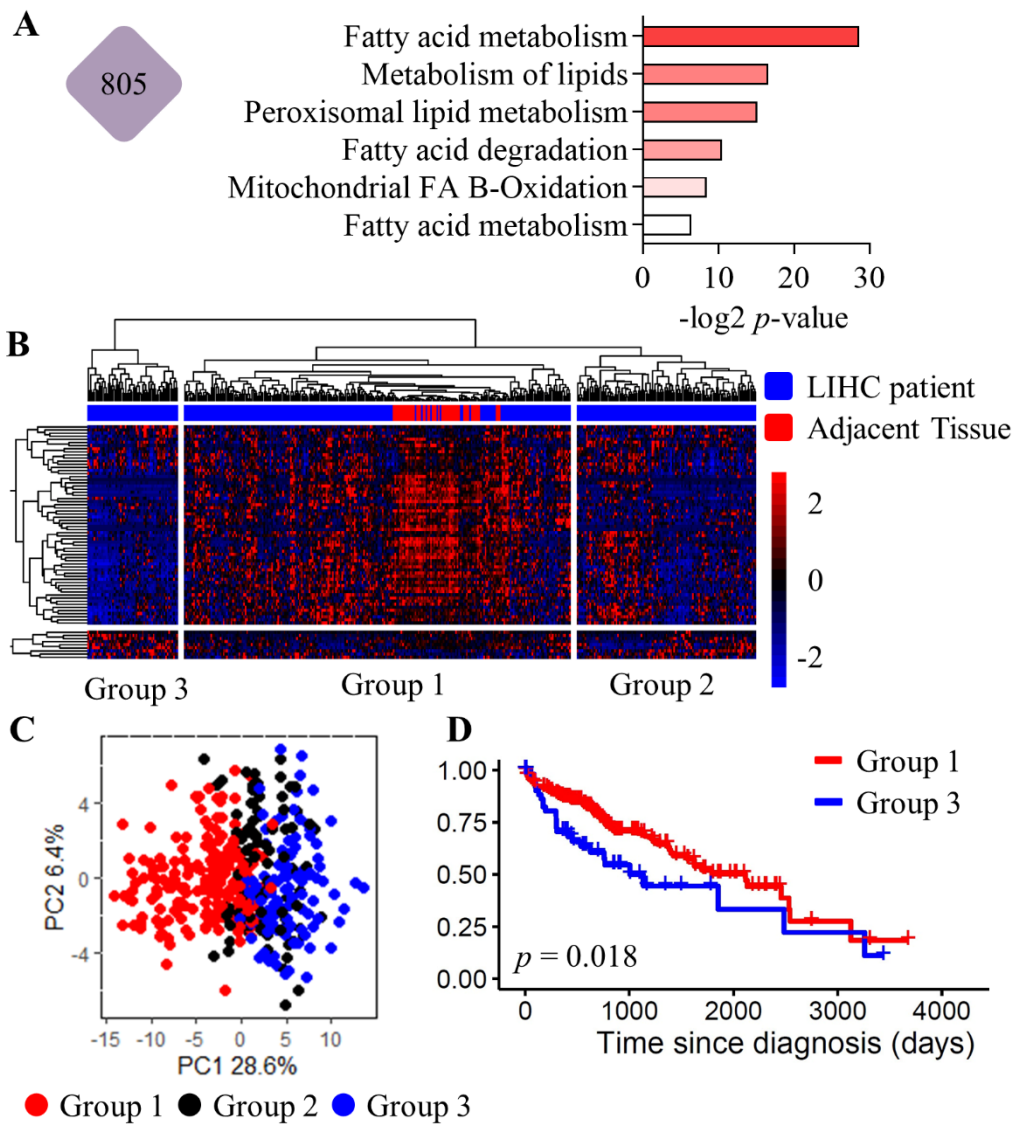


Figure 5. Lipid metabolism is suppressed in HCC and indicates severity of patients.

(A) Lipid related KEGG pathways were only enriched in 805 DEGs, upregulated in NAFLD and downregulated in HCC. (B) 371 HCC patients were clustered based on 73 lipids related DEGs based on spearman correlation. The clusters are divided into three groups based on expression patterns, where group 1 has high expression and similarity with adjacent normal tissue and group 3 has low expression. (C) PCA plot of group 1, 2 and 3

clearly distinguishes group 1 and 3. (D) Kaplan-Meier plot of patients in group 1 and group 3 suggests significantly low survival rate of group 3 than group 1. Significance is calculated with log-rank test.

6. DGAT2 expression follows patterns of lipid related DEGs

Since DGAT2 is in a part of 73 genes (Table 1), it is expected for DGAT2 to be upregulated in NAFLD and regressed in HCC patients. The spatial data of healthy, steatosis and HCC clearly demonstrates the expression of DGAT2 (Fig. 6A)^{24,25}. Comparison with H&E stained histology image with spatial data shows upregulated DGAT2 near ectopic fat regions in steatosis patients (Fig. 6B). This expression patterns are found from different cohort (GSE114564) (Fig. 6C). Moreover, DGAT2 expression decreases in group 3 (Fig. 6D). Notable point is that when comparing functional enrichments of DEGs from HepG2 DGAT2 inhibitory models, only DEGs in GO:CC mitochondrion exhibits similar pathways with downregulated DEGs in HCC patients (Fig. 6E). This implies that mitochondrial dysfunction mediated by DGAT2 inhibition mimics the pathways in HCC. To further observe DGAT2 expression patterns in various conditions. According to the clinical information in TCGA-LIHC project, DGAT2 expression is higher in female, but had no correlation with their etiology nor BMI (Fig. 7A-7C). This data might explain why mortality of male is higher than female. Different cohort (GSE193084) exhibits higher DGAT2 expression in NAFLD patients (Fig. 7D). Among various clinical categories, fibrosis is known to predict the outcomes of HCC, and DGAT2 expression negatively correlates with fibrosis stage (Fig. 7E). Additionally, the correlation of DGAT2 expression and HCC treatments were explored. Although sorafenib sensitive HCC patients show trend of decreased DGAT2 expression, there was no significance from sorafenib, Lenvatinib treatment, nor from recurrent tumor.

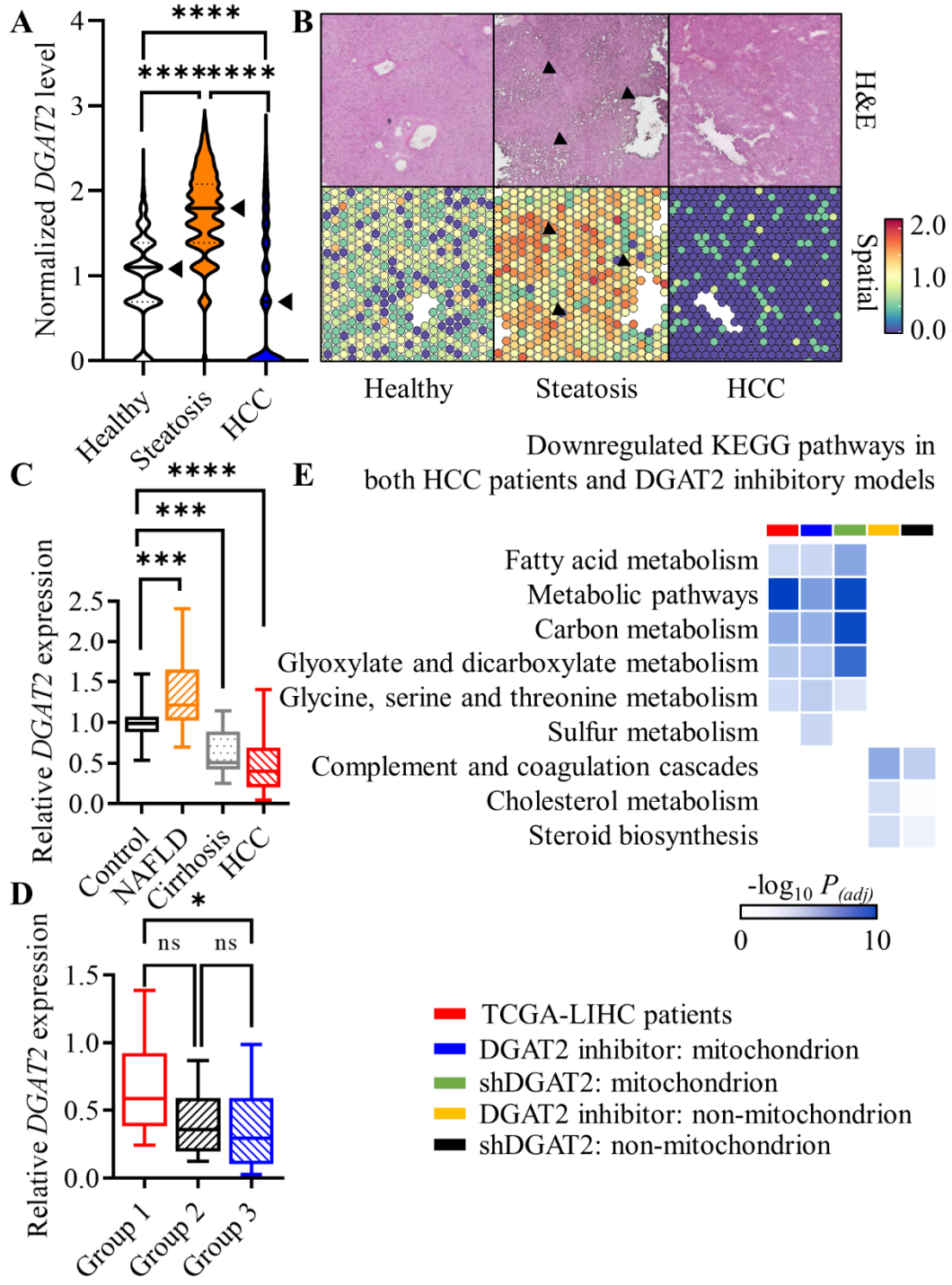


Figure 6. *DGAT2* expression regresses in HCC patients. (A) Normalized *DGAT2* expression value from healthy (n=2), steatosis (n=3) and HCC patients (n=4). Arrows indicate mean value of the plot. (B) Comparison of histology data with spatial expression data of *DGAT2* from healthy, steatosis and HCC patients. *DGAT2* level diminished in HCC patients. Arrows indicate steatosis area on steatosis patients, where *DGAT2* is highly expressed. (C) Relative *DGAT2* expression based on liver disease progression. Upregulated *DGAT2* expression in NAFLD decreases upon disease progression. (D) Relative *DGAT2* expression based on grouping of HCC patients. Group 3 shows lowest *DGAT2* expression level. (E) Transcriptome data of *DGAT2* inhibitory model suggests that downregulated DEGs in GO:CC Mitochondrion correlates with downregulated DEGs of HCC patients. Data represent mean + SD. *p<0.05, ***p<0.001, ****p<0.0001; Mann-Whitney U-test, two tailed. Gene enrichment data is calculated via FDR.

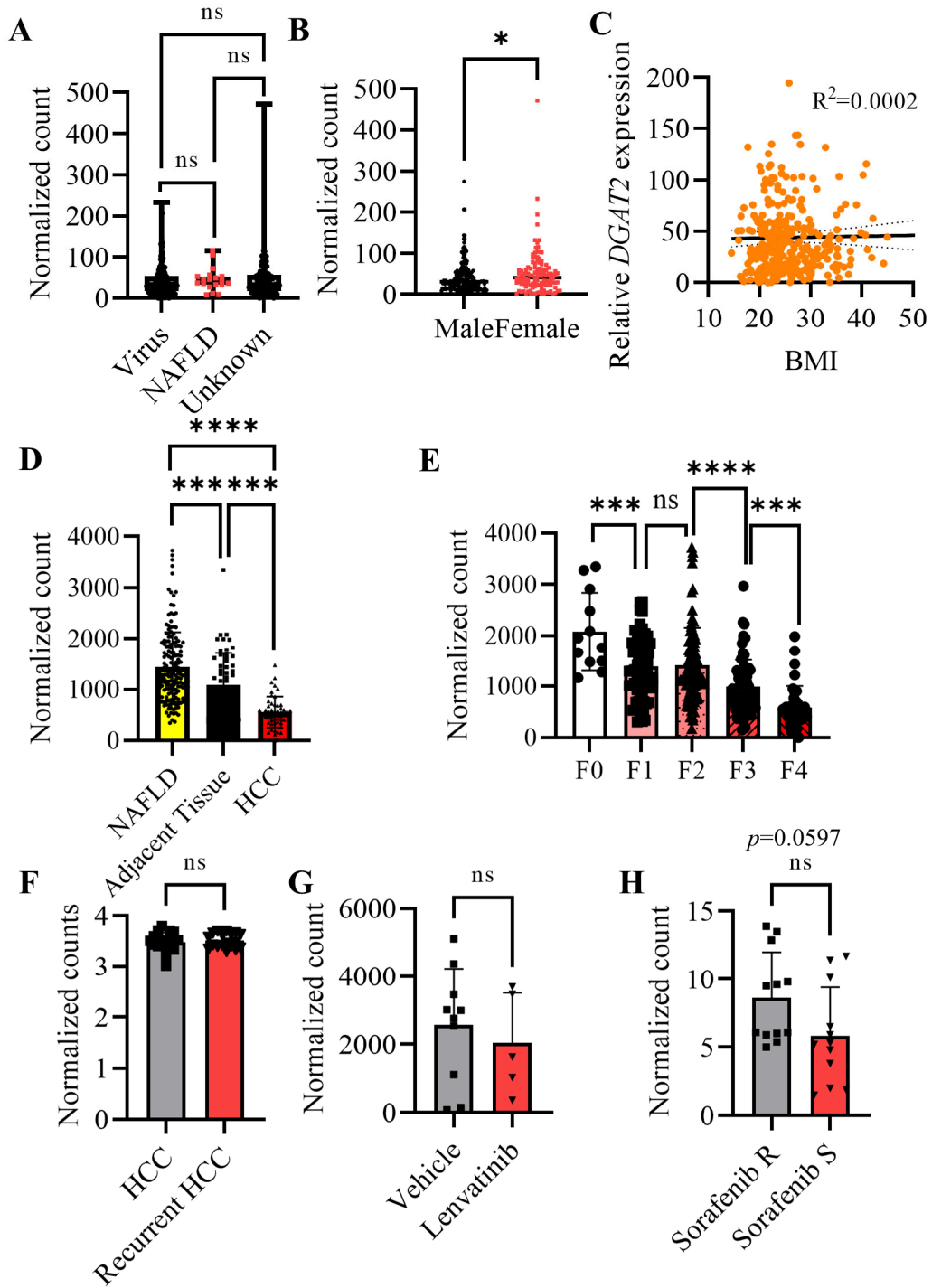


Figure 7. Correlation of *DGAT2* expression level and clinical variances in HCC patients. (A-C) Normalized *DGAT2* expression based on (A) etiology of patients from TCGA-LIHC samples suggests no differences. (B) Gender based expression shows higher expression in female. (C) Correlation with BMI suggest no significant differences. (D) Normalized *DGAT2* expression in different cohort based on liver disease progression suggest similar patterns. (GSE193084; NAFLD = 106, Tumor adjacent tissue = 59, HCC = 48). (E) Expression level based on fibrosis stage suggests gradual decrease of *DGAT2* expression. (F) Expression level of recurrent HCC show no difference with the first HCC (GSE164359; first HCC = 20, recurrent HCC = 27). (G) *DGAT2* expression does not changes upon Lenvatinib treatment. (GSE223201). (H) *DGAT2* expression of sorafenib sensitive and resistant tumor (GSE182593). Data represent mean + SD. * $p < 0.05$, *** $p < 0.001$, **** $p < 0.0001$; Mann-Whitney U-test, two tailed. Linear regression for (C).

7. Low DGAT2 expression correlates with poor HCC outcomes

The correlation of HCC stage and DGAT2 suggests negative correlation (Fig. 8A). Comprehensive consideration with previous data implies that patients with low DGAT2 patients are likely to face poor outcome. Thus, HCC patients from TCGA project were divided into high DGAT2 expressing group (n=100) and low DGAT2 expressing group (n=100) according to their normalized expression value (Fig. 8B). Although their PCA was not as significant as using 73 genes, low DGAT2 expression group exhibits lower survival probability as expected (Fig. 8C-8D). Moreover, low DGAT2 expressing group has differences in expression of genes regulating mitochondrial dynamics that STAT2, the gene for mitochondria biogenesis is suppressed while fission mediating DNM1L is upregulated in DGAT2 low group (Fig. 9A). Giving clue for the correlation of DGAT2 mitochondrial modifications in hepatoma.

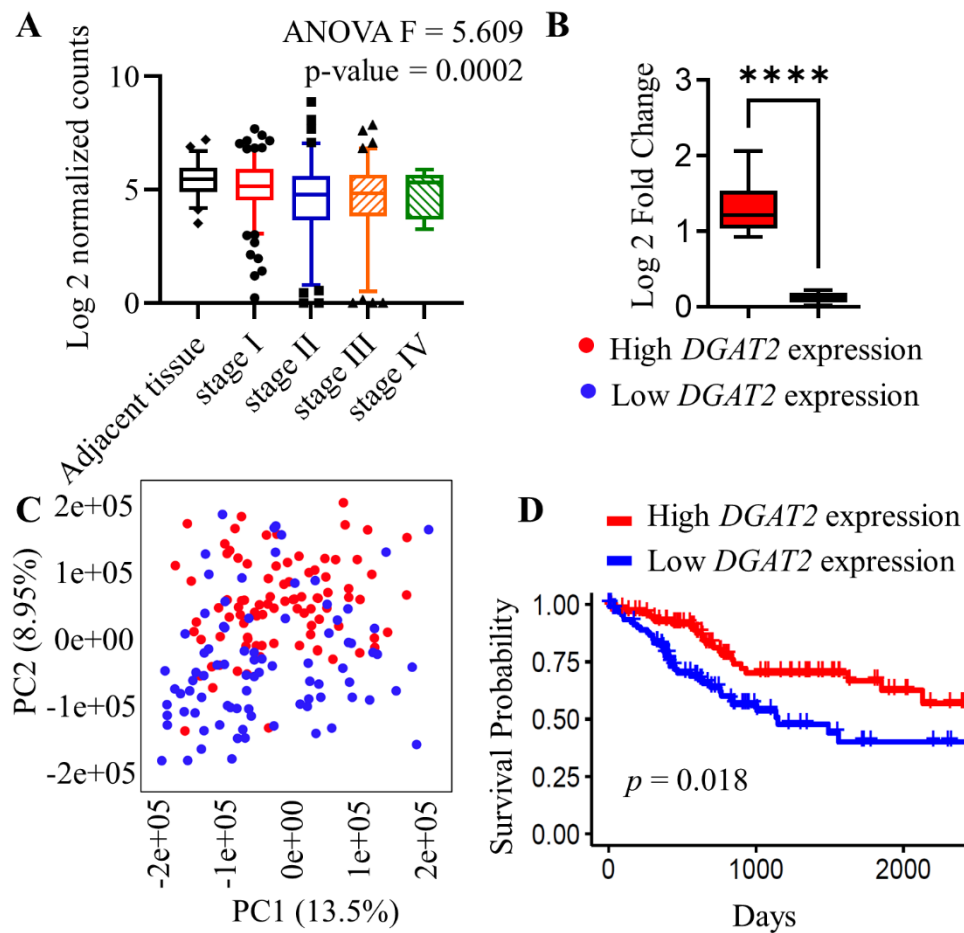


Figure 8. Low DGAT2 expressing HCC are more severe than high DGAT2 expressing HCC (A) Expression level of DGAT2 correlating to the HCC stage suggest severe HCC to express lower DGAT2 level. (B) DGAT2 expression level of high DGAT2 expressing group (n=100) and low DGAT2 expressing group (n=100). (C) PCA plot of HCC patients based of DGAT2 expression level. (D) Kaplan-Meier plot of DGAT2 high and low patients indicates low survival rate of low expressing group. Data represent mean + SD. **** $p < 0.0001$; Mann-Whitney U-test, two tailed. One-way ANOVA for (A). Log-rank test for (D).

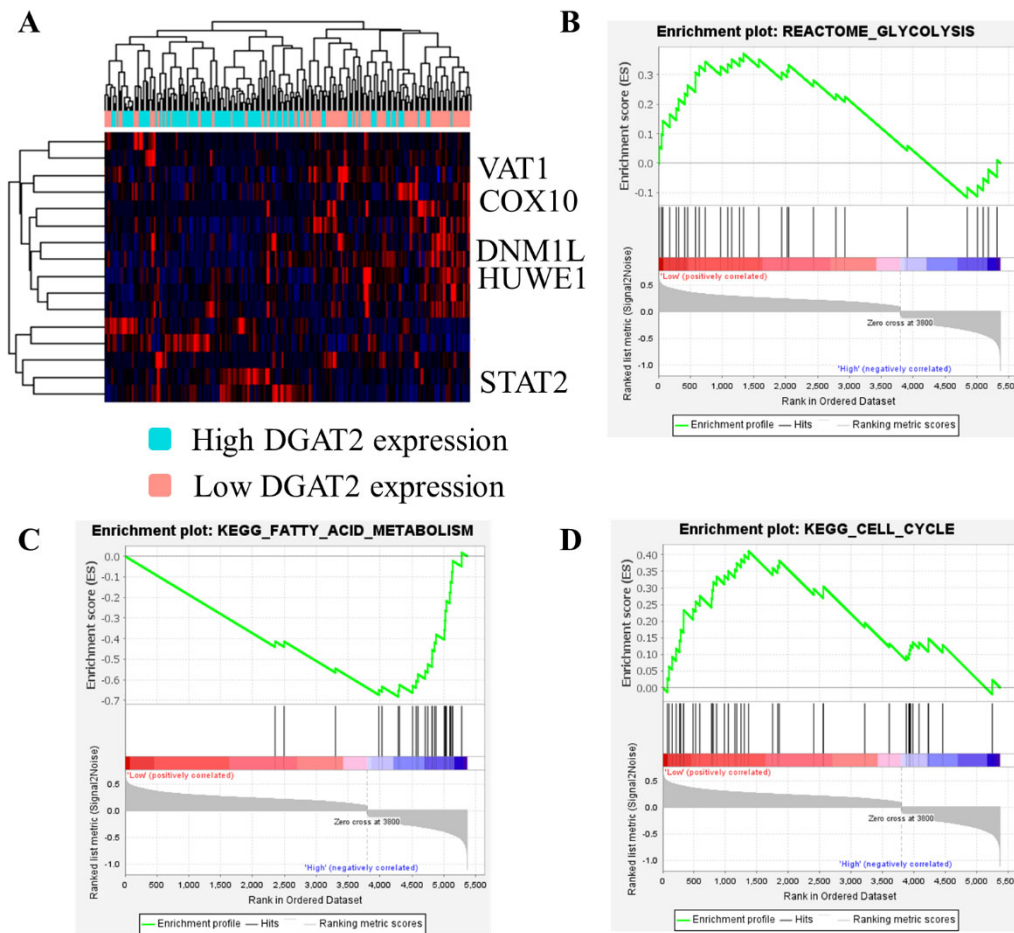


Figure 9. Metabolic differences in DGAT2 low HCC (A) Heatmap of mitochondria dynamics from DGAT2 high and low group. Fission regulators are upregulated. (B-D) GSEA data of shDGAT2 model (B) glycolysis is upregulated. (C) Fatty acid metabolism is downregulated. (D) Cell cycle is upregulated. Heatmap correlation is calculated with spearman correlation. Significance of GSEA is calculated with FDR.

8. DGAT2 inhibition via chemical inhibitor and shRNA reveals increased cellular proliferation and migration *in vitro*

Analyzing transcriptomes of DGAT2 KD cell suggests upregulation of glycolysis, and cell cycle while downregulation of fatty acid metabolism (Fig. 9B-9D). As GSEA clued the cell proliferation rate increases when DGAT2 is inhibited, and show statistically significant increases in day 3 (Fig. 10A). Although CCNB1 showed little differences, protein expression level of CDK2, CCNA2 and CCNE1 increased upon DGAT2 knockdown (Fig. 10B). These upregulation of proteins accelerates the cell cycle; therefore, S phase and G2 phase of DGAT2 KD cell line were increased (Fig. 10C). With the increased cellular proliferation of DGAT2 knockdown cell line, migration ability of DGAT2 KD cell line was increased. The wound closure assay suggests that migration ability is significantly upregulated and was able to find significant closure in day 3 (Fig. 10D-10E).

As cell requires sources for proliferation, glycolysis based on the Warburg effect was considered as a cancer adaptation. From DGAT2 inhibitory model, ECAR level and cellular lactate level is increased, indicates upregulated glycolysis (Fig. 11A-11B). Thus, by inhibiting glycolysis with 10 mM of 2-deoxy-glucose (2DG) treatment only reduced proliferation of DGAT2 KD cell line (Fig. 11C). However, there was no significance in hypoxic responses (Fig. 11D). To generalized the role of DGAT2 in other hepatoma, Hep3B cell line was compared with HepG2 cell line. Without any treatment, Hep3B has significantly low level of DGAT2 expression (Fig. 11E) Also, the cell proliferation rate of Hep3B is faster than HepG2 (Fig. 11F). Thus, inhibition of DGAT2 activity not only reduced TG accumulation but increases cell proliferation and migration speed via glycolysis.

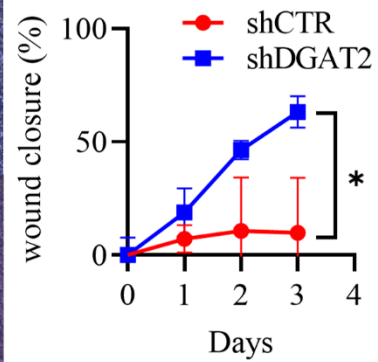
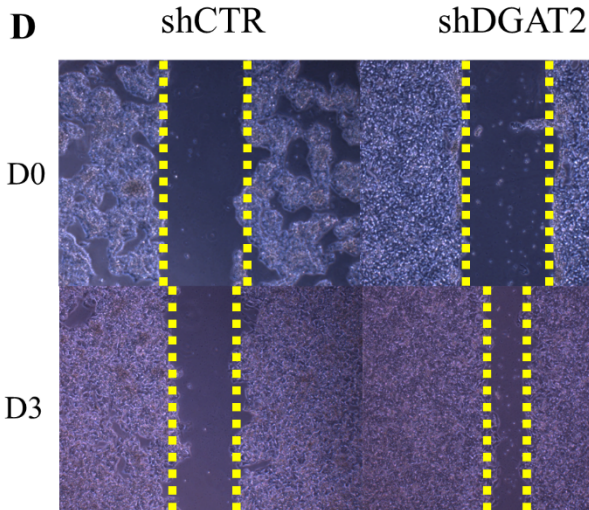
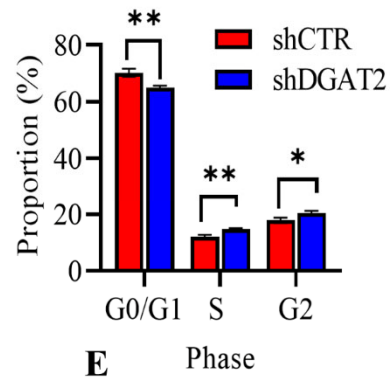
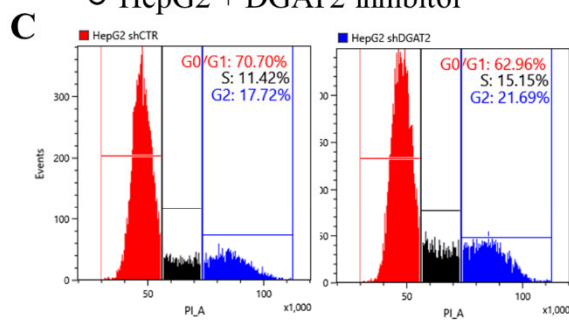
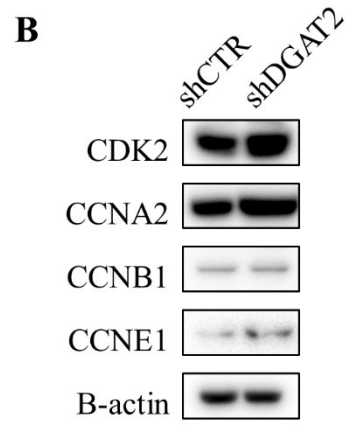
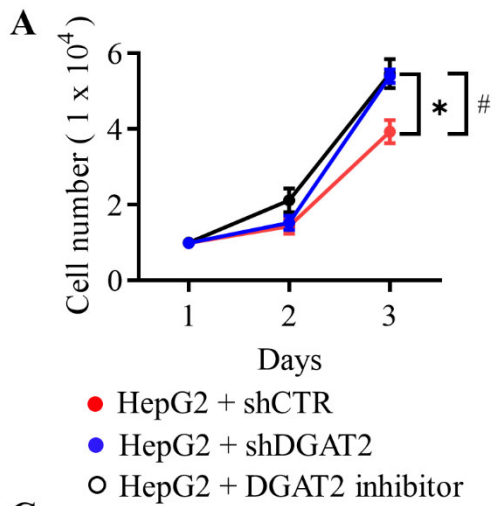


Figure 10. Cell proliferation and migration is upregulated in DGAT2 inhibitory model. (A) Cell proliferation rate after DGAT2 inhibition via knockdown and inhibitor. Asterisk indicates significance between control and knockdown model and pound indicates significance between control and inhibitor model. (B) Cell cycle dependent proteins appear to be upregulated in DGAT2 KD model. (C) Cell cycle assay via PI suggest higher proportion in S/G2 phase in DGAT2 KD model. (D) Wound healing assay to assess migration ability of cancer cell line. Microscopic images exhibit faster closure in DGAT2 KD model. (E) Relative percentage of wound closure measured with ImageJ. Data represent mean + SD. * $p < 0.05$, ** $p < 0.01$, # $p < 0.05$; student's t-test, two tailed.

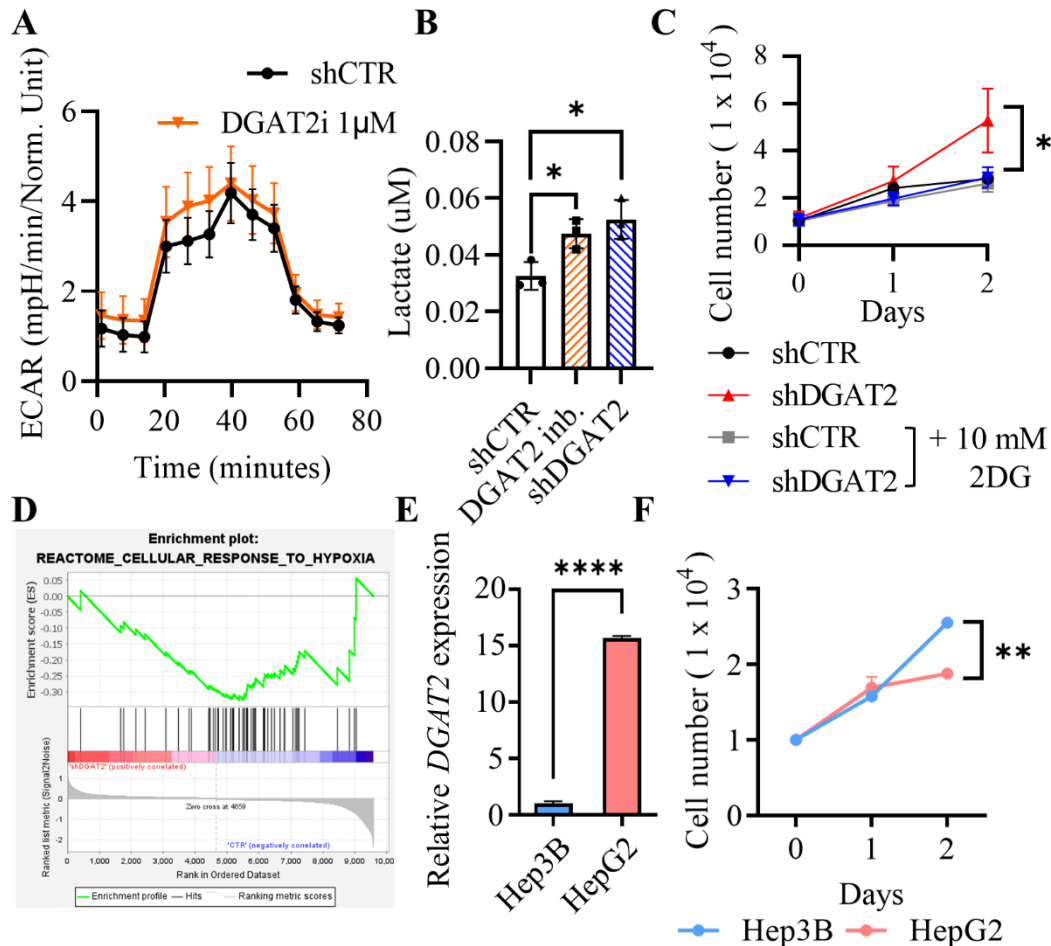


Figure 11. Glycolysis is upregulated in DGAT2 inhibitory model and promotes cell proliferation. (A) Glycolysis rate is measured with ECAR. (B) Cellular lactate level is measured to predict the abundance of glycolysis. (C) Cell proliferation after inhibiting glycolysis with 2DG infers glucose addiction of DGAT2 KD model. (D) DGAT2 KD model shows no significance in a cellular response to hypoxia. (E) DGAT2 expression level in different HCC cell line, Hep3B, is lower than that of HepG2. (F) Cell proliferation is faster in Hep3B cell line. Data represent mean + SD. * $p < 0.05$, ** $p < 0.01$, **** $p < 0.0001$; student's t-test, two tailed.

9. DGAT2 is more methylated in low DGAT2 expression group

To propose the likelihood for different *DGAT2* expression, genomic and epigenomic changes were assessed to understand the transcriptional change. To track the changes in *DGAT2* expression, *DGAT2* expression level from paired adjacent tissue and tumor tissue is compared. The graph suggests that the expression level shows no significant differences in adjacent tissues, while their tumor shows significant increases and decreases in *DGAT2* expression (Fig. 12A). It suggests that changes in *DGAT2* expression during normal to tumor transition determines the eventual expression level of *DGAT2*. First, the methylation intensity of CpG island of *DGAT2* region was compared. According to the patients in TCGA LIHC cohort, *DGAT2* low expressing patients have more intense methylation on *DGAT2* region (Fig. 12B). However, there was no difference in the copy number of *DGAT2* (Fig. 12C). Also, to confirm whether *DGAT2* is mutated in HCC patients, the mutation data was checked. *DGAT2* mutation is known to be a cause of Charcot-Marie disease. However, mutation was not always the case of HCC that more than 9,000 genes are mutated in less than 1 % of HCC patients (Fig. 12D). For *DGAT2*, only 2 patients are confirmed to have mutation, yet is a silent mutation¹⁸ (Table. 2). Therefore, it would be rational to consider that methylation would be a major driver to control *DGAT2* expression.

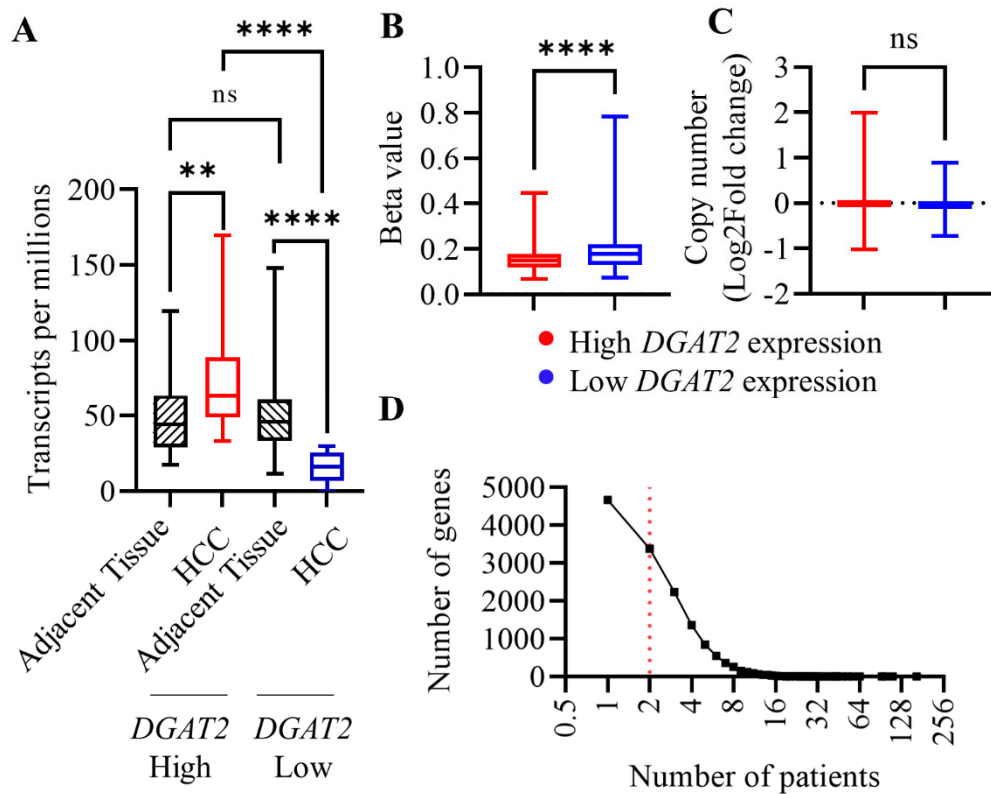


Figure 12. Genomic analysis suggest methylation to be a regulator of DGAT2 expression. (A) DGAT2 expression of paired HCC patients with their adjacent tissue (TCGA-LIHC; adjacent tissue =50, HCC = 50). Initial DGAT2 levels in normal tissue in DGAT2 high and low groups have no differences. (B) Methylation level on CpG island of DGAT2 genomic region is higher in DGAT2 low expressing group. (C) Copy number of DGAT2 gene has no differences. (D) Probability of DGAT2 mutation is very low that only 2 patients possess mutated DGAT2 gene. Data represent mean + SD. ** $p < 0.01$, **** $p < 0.0001$; Mann Whitney U-test, two tailed.

Table 2. List of patients from TCGA LIHC cohort with DGAT2 mutation

Patients	Gene	SNP
TCGA-DD-A4NQ	DGAT2	Silent
TCGA-DD-A1EA	DGAT2	Silent

10. ESRRA signal is downregulated when DGAT2 is inhibited

It is observed that DGAT2 inhibition promotes mitochondrial dysfunction. However, little is known to discover the linkage between DGAT2 and mitochondria. Therefore, to find clue transcriptome data is performed ISMARA for assessing motif activities²⁶. By comparing the gene expression and motifs in promoter region, ISMARA calculates the potential activity of motifs. Within top 10 motifs, motifs for PLAGL1, ESRRA, and KLF16 was showing similar activity patterns with DGAT2 expression (Fig. 13A). Among three of motifs, ESRRA are also detected in transcriptome of DGAT2 inhibitor treated HepG2 and DGAT2 knockdown models (Fig. 13B-13C). Thus, the activity of ESRRA is tested with luciferase assay using ERRE motif, which gives more than 50% decrease in luciferase activity (Fig. 13D). To check the chromatin accessibility of DGAT2 knockdown HepG2, Assay for Transposase-Accessible Chromatin with high-throughput sequencing (ATAC sequencing) is performed²⁷. When comparing the openness of chromatin structure, ESRRA motif is seems to have higher peak count frequency (Fig. 13E), which explains the downregulation of genes with ERRE sequences in promoter regions (Fig. 13F).

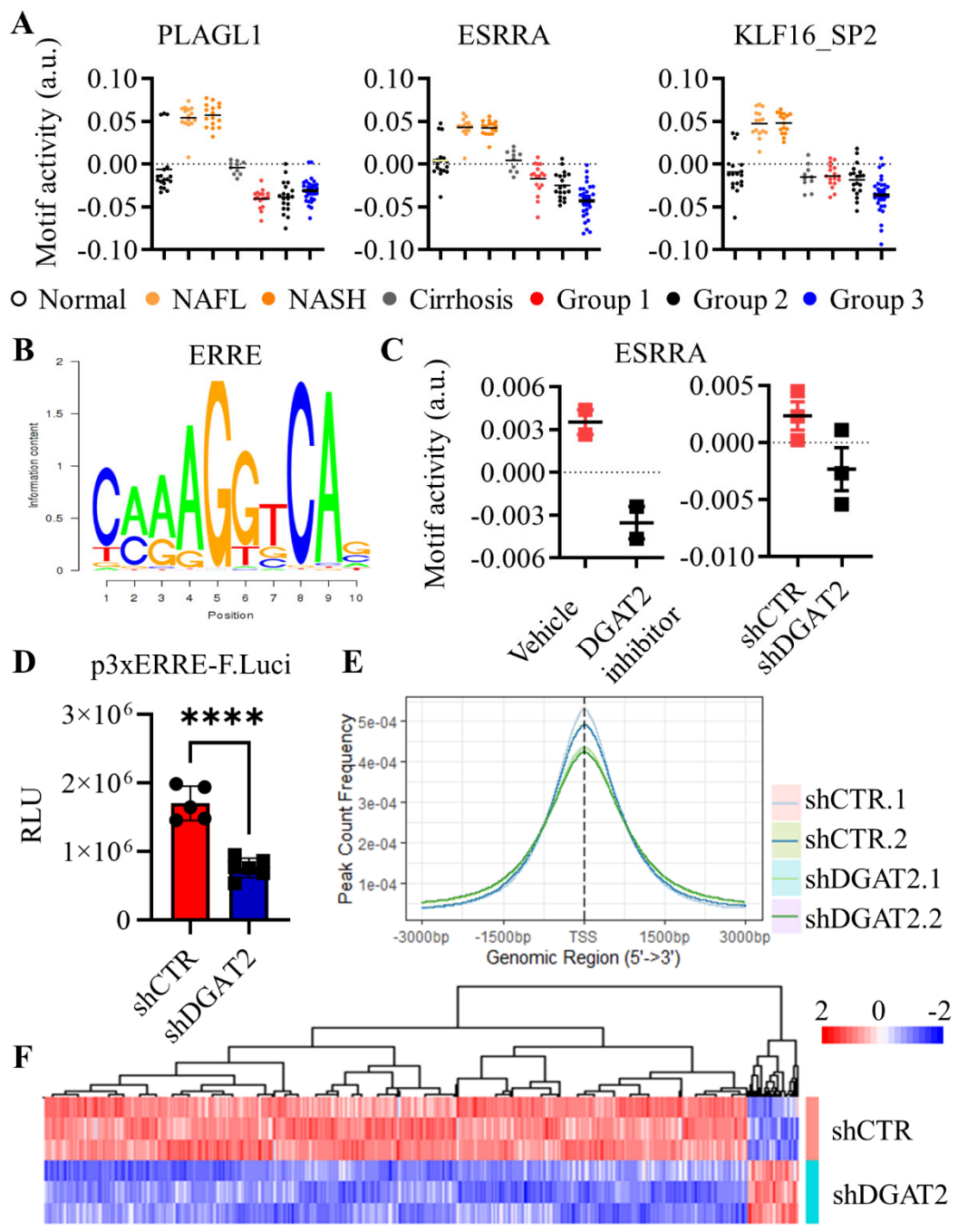


Figure 13. ESRRA motif, ERRE, is suppressed in DGAT2 KD model. (A) ISMARA based calculation predicted motifs for PLAGL1, ESRRA, and KLF16_SP2 follows similar patterns with DGAT2 expression in liver diseases. (B) Image of motif sequence of ESRRA, ERRE. (C) Motif activity of ESRRA in DGAT2 inhibitory model. (D) Luciferase assay to test motif activity in DGAT2 KD model suggest suppressed activity. (E) ATAC sequencing analysis suggests fewer peak counts on ERRE site in DGAT2 KD model. (F) Transcriptome data exhibits downregulation of genes with ERRE motif on their promoter regions. Data represent mean + SD. ** $p < 0.01$, *** $p < 0.0001$; student's t-test, two tailed. Significance of ISMARA is calculated with z-values.

11. ESRRA-PROX1 transcriptional network is suppressing the ESRRA signal

ESRRA works as a transcription factor with cofactors. PPARGC1A(PGC1A)²⁸ binds for activation, while PROX1²⁹ binds for repression. To analyze activity of ESRRA, cofactors were assayed and found PGC1A to be decreased while PROX1 is upregulated in DGAT2 KD sample (Fig. 14A). Next, subfraction was performed for protein detection. Among two cofactors of ESRRA, PGC1A and PROX1, only PROX1 was detected in nucleus with ESRRA (Fig. 14B). To confirm the expression level of Thus, nucleus fraction is used for immunoprecipitation with a bait, ESRRA. IP data gives that PROX1 which work as a repressor binds more intensively to ESRRA when DGAT2 is knockdown (Fig. 14C). These data suggest not only the expression of ESRRA decreases, PROX1 binds more on ESRRA to create suppressive transcriptional network in hepatoma. Another possibility includes endogenous ligand, cholesterol and ESRRA activator protein kinase C epsilon (PKC ϵ). However, the level of cholesterol level is not changed (Fig. 14D). Although DAG, ligand of PKC family, level shows trends of decreasing (p=0.2) and phosphatidic acid, products from DAG, level increased in DGAT2 KD sample (Fig. 14F). There is no significance. Yet, the protein level of PKC ϵ decreased and might explain the loss of ESRRA activity (Fig. 14G).

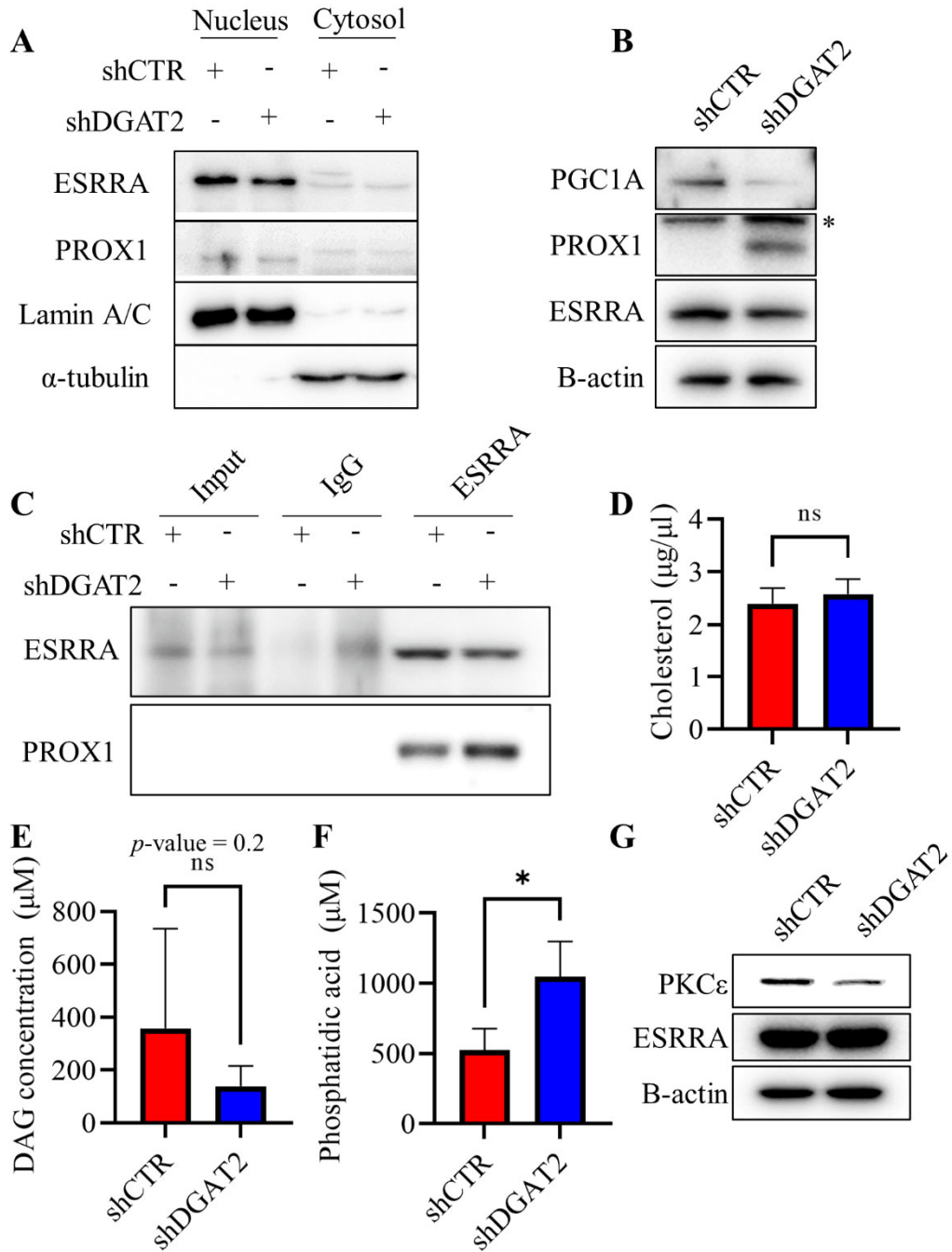
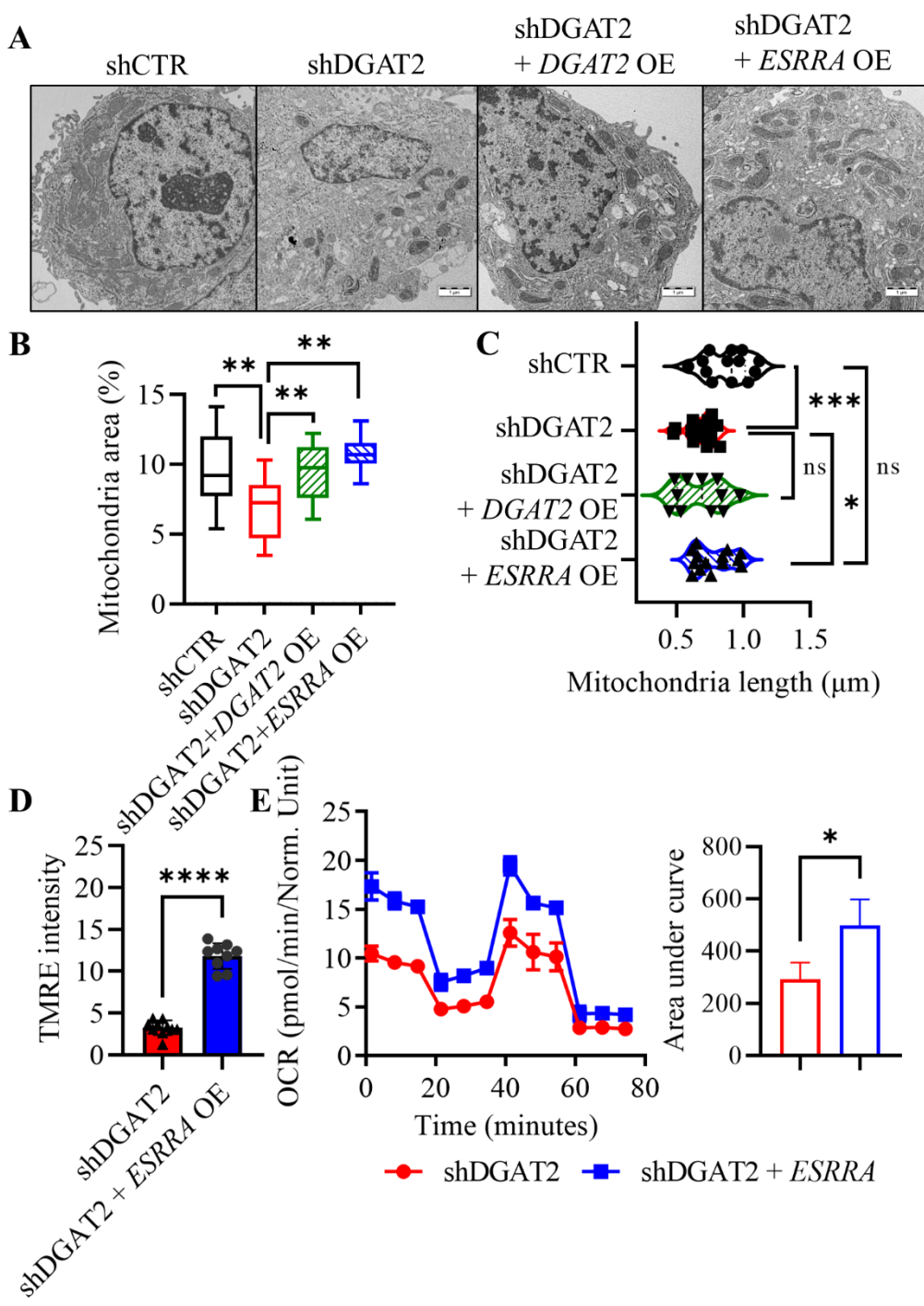


Figure 14. ESRRRA cofactors suppress ESRRRA activity. (A) Protein levels of ESRRRA cofactors show PGC1A, coactivator, to be suppressed in DGAT2 KD model while PROX1, corepressor, is upregulated. (B) ESRRRA and cofactors are located in nucleus. (C) IP assay suggests ESRRRA-PROX1 interaction is increased in DGAT2 KD model. (D) Cholesterol level, endogenous ESRRRA ligand, shows no differences. (E) DAG level shows no significant differences, while (F) phosphatidic acid derived from DAG increased. (G) ESRRRA activator, PKC ϵ is decreased in DGAT2 KD model. Data represent mean + SD. * $p < 0.05$; student's t-test, two tailed.

12. Mitochondrial dysfunction is rescued with *ESRRA* overexpression

To confirm whether *ESRRA* is a key transcription factor working in *DGAT2* inhibited HCC, *ESRRA* is overexpressed to *DGAT2* knockdown HepG2 cell line. The overexpression of both *DGAT2* and *ESRRA* on HepG2 *DGAT2* KD cell line recovered mitochondrial morphology, including area, length, and membrane potential.(Fig. 15A-15D). As the morphology recovers, OCR is rescued (Fig. 15E). Moreover, mitochondria restoration via *ESRRA* OE suppresses cell proliferation (Fig. 15F). To further investigate the network of *ESRRA*-*PROX1*, *PROX1* is knockdown with shRNA and cell proliferation was tested. As expected, cell proliferation is decreased in *PROX1* KD and *DGAT2* KD cell line (Fig. 15G).



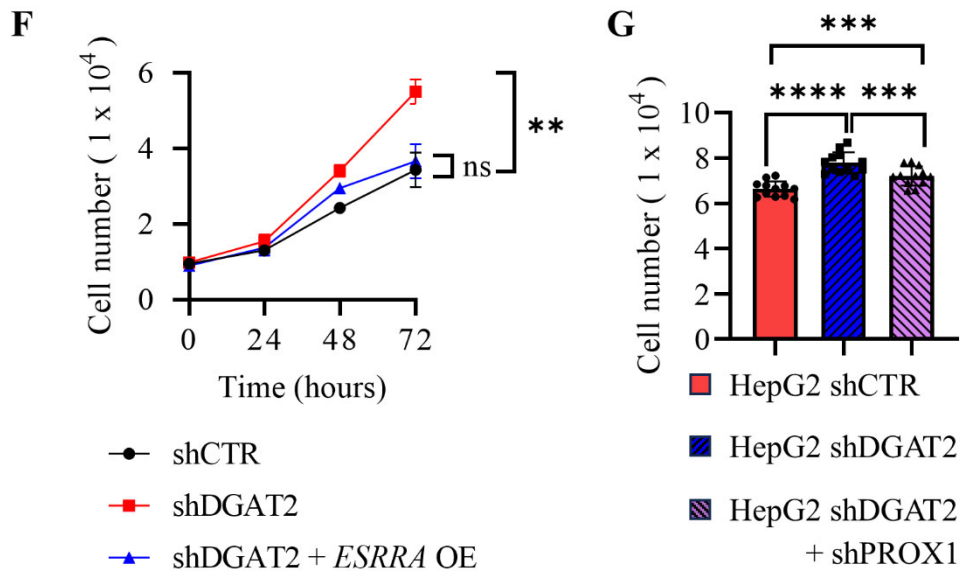


Figure 15. Overexpression of *ESRRR* rescues mitochondrial function and cell proliferation. (A) TEM images of HepG2 models. Dark gray organelle in cytosol indicates mitochondria. (B) Mitochondrial area is measured with ImageJ, relative to cytosol area, and exhibits increased area upon *DGAT2* and *ESRRR* overexpression. (C) Mitochondrial length is rescued with *ESRRR* overexpression. (D) Mitochondrial potential, measured with TMRE intensity, increased with *ESRRR* overexpression. (E) OCR increased via *ESRRR* overexpression. (F) Cell proliferation rate after *ESRRR* overexpression rescued induced proliferation. (G) *PROX1* knockdown suppresses cell proliferation of *DGAT2* KD model. Data represent mean + SD. * $p < 0.05$, ** $p < 0.01$, *** $p < 0.001$, **** $p < 0.0001$; student's t-test, two tailed.

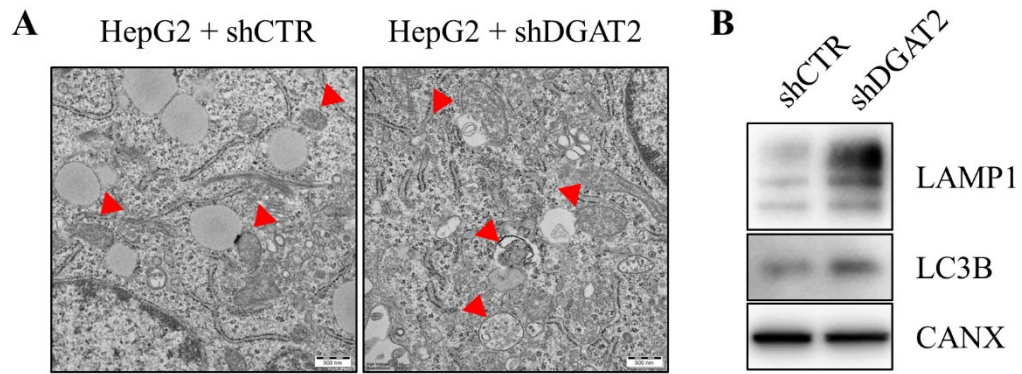


Figure 16. Mitophagy is promoted in DGAT2 KD model. (A) TEM images of DGAT2 KD model. Red arrow indicates mitochondria in cytosol. DGAT2 KD model exhibits mitophagy. (B) Proteins inducing autophagosome formation are upregulated in ER.

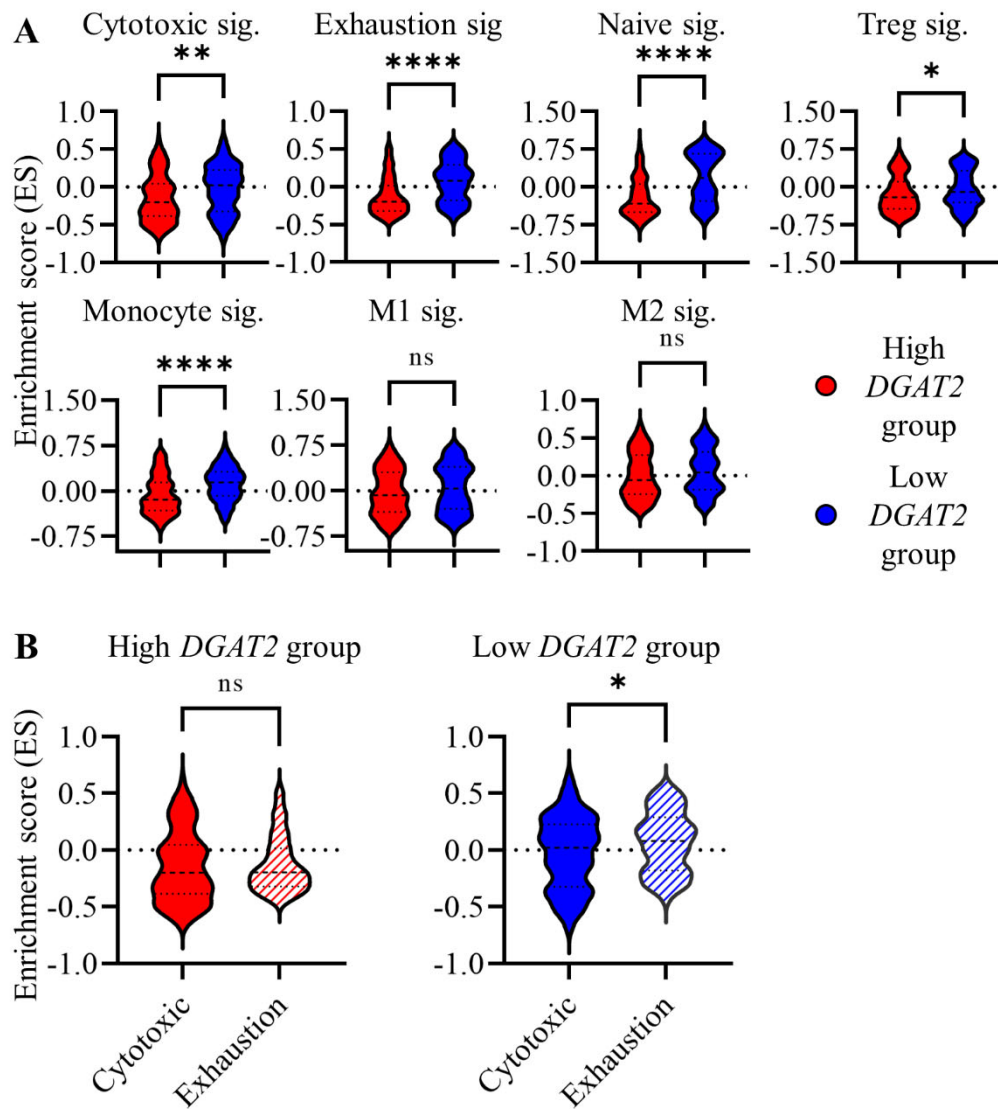


Figure 17. Correlation of immune function with DGAT2 expression level. (A) Immune signatures were calculated from HCC patients using ssGSEA. Despite the pro- or anti-inflammatory functions low DGAT2 group exhibits higher scores. (B) Comparison of exhaustion score relative to cytotoxic score suggests low DGAT2 group to have more exhausted immune functions. Data represent mean + SD. * $p < 0.05$, ** $p < 0.01$, **** $p < 0.0001$; Mann Whitney U-test, two tailed.

IV. DISCUSSION

Metabolism shift in the cancer is a common and a strong adaptation for cancer survival. Cancers can utilize metabolites including glucose, amino acids, and lipid³⁰. Due to diversity of lipid species and its abundancy, the role of lipid in hepatocellular carcinoma is yet to be clarified³¹. Moreover, as a metabolic organ, liver itself exhibits strong heterogeneous characteristics. Therefore, subtyping to categorizing liver cancers were held since 2007³²⁻³⁴. Some clusters HCC into a proliferative to non-proliferative cancers, while the other clusters with genomic mutation level or the abundance of immune cells. Among those categorizations, it was a first attempt to find difference in liver cancer in terms of lipid metabolism.

Major etiologies of HCC are HBV, HCV, and NAFLD. Since each disease has distinct pathogenesis, the metabolic differences in HCC mediated from each diseases need to be accounted. However, it is hard to roll out the consequences of a single etiology in HCC due to their abundancy in patients. Each patient possesses multiple etiologies that considering TCGA database of LIHC patients, the number of patients with single etiology is 43, 20, and 7 for HBV, HCV, and NAFLD respectively. Moreover, the observational studies on survival rate of HCC patients with different etiology exhibits conflicting results. One claims etiology does not change the survival rate of the patients and the other claims HBV-mediated HCC patients show the better survival rate than the others³⁵. Nevertheless, one significant factor causing low survival rate is the low awareness toward HCC¹⁰, which correlates with the data that patients with family history of HCC sustains higher survival rates³⁶. Thus, if *DGAT2* expression level decreases from its adjacent tissue, patients require more awareness toward the HCC.

Considering that DGAT2 converts DAG and Acyl-CoA into TG, DGAT2 inhibition would force the decrease in TG while unused DAG will keep increasing in hepatocytes. While blood is a favorable source from patients, lowering TG from HCC patients are reported³⁷ previously. However, the level of DAG in serum is not reported in HCC patients. According to the DAG assay from DGAT2 inhibited HepG2 cell, it is shown that DAG level is not changed, hence shows tendency to be decreased rather than increased DAG level due to DGAT2 inhibition. In contrast the level of phosphatidic acid (PA), a metabolite derived from DAG, is increased in DGAT 2 inhibited HepG2³⁸. Thus, the low level of TG and DAG with increased PA in serum could be a metabolic marker for HCC patients.

While mitochondrial dysfunction is well known to be a hallmark of a cancer, it is still vague how it directly promotes tumor progression. Considering the increased cell proliferation, cells require more energy and building blocks to sustain the growth. Despite the glycolysis, TEM images suggest mitophagy from DGAT2 KD cell line (Fig 16A). Moreover, the expression of LC3B and LAMP1 is highly increased in mitochondria, which recruits autophagosome (Fig 16B).

Immune response in tumor microenvironments regulates the growth and survival rate of tumor and immune evasion is considered as a key factor in cancer hallmarks. Little is known about the correlations between DGAT2 and immune function in cancer. Moreover, the controversy perspectives of immune response in NAFLD and HCC make it harder to comprehend that in NAFLD, anti-immune functions are considered as a positive marker where in HCC, pro-immune functions are considered as safer. Based on immune signature, pro- and anti-

immune activities are scored⁴². The enrichment score suggests both pro-inflammatory signature, naïve and cytotoxic signatures, and anti-inflammatory signature, exhaustion, and regulatory T cell signatures, are upregulated in low DGAT2 group (Fig. 17A). Therefore, considering single factor make it hard to interpret the correlation of DGAT2 and immune function. However, comparing the cytotoxic signature with exhaustion signature, only low DGAT2 group exhibits significantly increased exhaustion signature than cytotoxic signature (Fig. 17B).

In the consideration of DGAT2 inhibition, the TG precursor, diacylglycerol (DAG) needs to be accounted for its lipotoxicity and protein kinase C activation³⁹. Moreover, considering there is a report that PKC activation downregulates ESRRA activity, which eventually promotes HCC⁴⁰. Nevertheless, PROX1 itself is reported to promote cell proliferation⁴¹, which leads to the possibilities that DGAT2 inhibition initiates multiples transcriptional activation parallelly.

V. CONCLUSION

Overall data illustrate that transcriptional network of ESRRA-PROX1 is induced in the absence of DGAT2 activity, which leads to the loss of mitochondrial function in hepatoma. When DGAT2 activity is suppressed, ESRRA-PROX1 transcriptomic network is upregulated and suppress ESRRA activity. Following with the downregulation of STAT2 and Drp1 like mitochondria dynamic associated genes, mitochondria will lose its functions such as TCA cycle. Then the glycolysis pathway is upregulated to provide energies for cell proliferation. Thus, DGAT2 can be considered as a regulator in hepatoma to sustain mitochondrial function along with its well-known function, TG synthesis.

REFERENCES

1. Rumgay H, Arnold M, Ferlay J, Lesi O, Cabasag CJ, Vignat J, et al. Global burden of primary liver cancer in 2020 and predictions to 2040. *J Hepatol* 2022;77:1598-606.
2. Siegel RL, Miller KD, Wagle NS, Jemal A. Cancer statistics, 2023. *CA Cancer J Clin* 2023;73:17-48.
3. Schaffner F, Thaler H. Nonalcoholic fatty liver disease. *Prog Liver Dis* 1986;8:283-98.
4. Sunami Y. NASH, Fibrosis and Hepatocellular Carcinoma: Lipid Synthesis and Glutamine/Acetate Signaling. *Int J Mol Sci* 2020;21.
5. Dyson J, Jaques B, Chattopadhyay D, Lochan R, Graham J, Das D, et al. Hepatocellular cancer: the impact of obesity, type 2 diabetes and a multidisciplinary team. *J Hepatol* 2014;60:110-7.
6. Huang DQ, El-Serag HB, Loomba R. Global epidemiology of NAFLD-related HCC: trends, predictions, risk factors and prevention. *Nat Rev Gastroenterol Hepatol* 2021;18:223-38.
7. Pei K, Gui T, Kan D, Feng H, Jin Y, Yang Y, et al. An Overview of Lipid Metabolism and Nonalcoholic Fatty Liver Disease. *Biomed Res Int* 2020;2020:4020249.
8. Sanyal A, Poklepovic A, Moyneur E, Barghout V. Population-based risk factors and resource utilization for HCC: US perspective. *Curr Med Res Opin* 2010;26:2183-91.
9. Loomba R, Lim JK, Patton H, El-Serag HB. AGA Clinical Practice Update on Screening and Surveillance for Hepatocellular Carcinoma in Patients With Nonalcoholic Fatty Liver Disease: Expert Review. *Gastroenterology*

- 2020;158:1822-30.
10. Younes R, Bugianesi E. Should we undertake surveillance for HCC in patients with NAFLD? *J Hepatol* 2018;68:326-34.
 11. Fahy E, Cotter D, Sud M, Subramaniam S. Lipid classification, structures and tools. *Biochim Biophys Acta* 2011;1811:637-47.
 12. Nakagawa H, Hayata Y, Kawamura S, Yamada T, Fujiwara N, Koike K. Lipid Metabolic Reprogramming in Hepatocellular Carcinoma. *Cancers (Basel)* 2018;10.
 13. Grbcic P, Car EPM, Sedic M. Targeting Ceramide Metabolism in Hepatocellular Carcinoma: New Points for Therapeutic Intervention. *Curr Med Chem* 2020;27:6611-27.
 14. Esler WP, Bence KK. Metabolic Targets in Nonalcoholic Fatty Liver Disease. *Cell Mol Gastroenterol Hepatol* 2019;8:247-67.
 15. Yen CL, Stone SJ, Koliwad S, Harris C, Farese RV, Jr. Thematic review series: glycerolipids. DGAT enzymes and triacylglycerol biosynthesis. *J Lipid Res* 2008;49:2283-301.
 16. Futatsugi K, Kung DW, Orr ST, Cabral S, Hepworth D, Aspnes G, et al. Discovery and Optimization of Imidazopyridine-Based Inhibitors of Diacylglycerol Acyltransferase 2 (DGAT2). *J Med Chem* 2015;58:7173-85.
 17. Choi CS, Savage DB, Kulkarni A, Yu XX, Liu ZX, Morino K, et al. Suppression of diacylglycerol acyltransferase-2 (DGAT2), but not DGAT1, with antisense oligonucleotides reverses diet-induced hepatic steatosis and insulin resistance. *J Biol Chem* 2007;282:22678-88.
 18. Graber M, Barta H, Wood R, Pappula A, Vo M, Petreaca RC, et al. Comprehensive Genetic Analysis of DGAT2 Mutations and Gene Expression Patterns in Human Cancers. *Biology (Basel)* 2021;10.

19. Raudvere U, Kolberg L, Kuzmin I, Arak T, Adler P, Peterson H, et al. g:Profiler: a web server for functional enrichment analysis and conversions of gene lists (2019 update). *Nucleic Acids Res* 2019;47:W191-W8.
20. Love MI, Huber W, Anders S. Moderated estimation of fold change and dispersion for RNA-seq data with DESeq2. *Genome Biol* 2014;15:550.
21. Stone SJ, Levin MC, Zhou P, Han J, Walther TC, Farese RV, Jr. The endoplasmic reticulum enzyme DGAT2 is found in mitochondria-associated membranes and has a mitochondrial targeting signal that promotes its association with mitochondria. *J Biol Chem* 2009;284:5352-61.
22. Rowland AA, Voeltz GK. Endoplasmic reticulum-mitochondria contacts: function of the junction. *Nat Rev Mol Cell Biol* 2012;13:607-25.
23. Reimand J, Kull M, Peterson H, Hansen J, Vilo J. g:Profiler--a web-based toolset for functional profiling of gene lists from large-scale experiments. *Nucleic Acids Res* 2007;35:W193-200.
24. Wu R, Guo W, Qiu X, Wang S, Sui C, Lian Q, et al. Comprehensive analysis of spatial architecture in primary liver cancer. *Sci Adv* 2021;7:eabg3750.
25. Habenicht LKL, Wang Z, Zhang X, Li Y, Mogler C, Huspenina JS, et al. The C1q-ApoE complex: A new hallmark pathology of viral hepatitis and nonalcoholic fatty liver disease. *Frontiers in Immunology* 2022;13.
26. Balwierz PJ, Pachkov M, Arnold P, Gruber AJ, Zavolan M, van Nimwegen E. ISMARA: automated modeling of genomic signals as a democracy of regulatory motifs. *Genome Res* 2014;24:869-84.
27. Yan F, Powell DR, Curtis DJ, Wong NC. From reads to insight: a hitchhiker's guide to ATAC-seq data analysis. *Genome Biol* 2020;21:22.
28. Charos AE, Reed BD, Raha D, Szekely AM, Weissman SM, Snyder M. A highly integrated and complex PPARGC1A transcription factor binding

- network in HepG2 cells. *Genome Res* 2012;22:1668-79.
29. Charest-Marcotte A, Dufour CR, Wilson BJ, Tremblay AM, Eichner LJ, Arlow DH, et al. The homeobox protein Prox1 is a negative modulator of ERRalpha/PGC-1alpha bioenergetic functions. *Genes Dev* 2010;24:537-42.
 30. Sangineto M, Villani R, Cavallone F, Romano A, Loizzi D, Serviddio G. Lipid Metabolism in Development and Progression of Hepatocellular Carcinoma. *Cancers (Basel)* 2020;12.
 31. Li C, Li L, Lian J, Watts R, Nelson R, Goodwin B, et al. Roles of Acyl-CoA:Diacylglycerol Acyltransferases 1 and 2 in Triacylglycerol Synthesis and Secretion in Primary Hepatocytes. *Arterioscler Thromb Vasc Biol* 2015;35:1080-91.
 32. Boyault S, Rickman DS, de Reynies A, Balabaud C, Rebouissou S, Jeannot E, et al. Transcriptome classification of HCC is related to gene alterations and to new therapeutic targets. *Hepatology* 2007;45:42-52.
 33. Delis SG, Bakoyiannis A, Tassopoulos N, Athanassiou K, Kechagias A, Kelekis D, et al. Hepatic resection for large hepatocellular carcinoma in the era of UCSF criteria. *HPB (Oxford)* 2009;11:551-8.
 34. Wu Y, Liu Z, Xu X. Molecular subtyping of hepatocellular carcinoma: A step toward precision medicine. *Cancer Commun (Lond)* 2020;40:681-93.
 35. Brar G, Greten TF, Graubard BI, McNeel TS, Petrick JL, McGlynn KA, et al. Hepatocellular Carcinoma Survival by Etiology: A SEER-Medicare Database Analysis. *Hepatology* 2020;4:1541-51.
 36. Aljumah AA, Kuriry H, AlZunaitan M, Al Ghobain M, Al Muaikeel M, Al Olayan A, et al. Clinical Presentation, Risk Factors, and Treatment Modalities of Hepatocellular Carcinoma: A Single Tertiary Care Center Experience. *Gastroenterol Res Pract* 2016;2016:1989045.

37. Liu X, Li M, Wang X, Dang Z, Jiang Y, Wang X, et al. Effect of serum triglyceride level on the prognosis of patients with hepatocellular carcinoma in the absence of cirrhosis. *Lipids Health Dis* 2018;17:248.
38. Cai J, Abramovici H, Gee SH, Topham MK. Diacylglycerol kinases as sources of phosphatidic acid. *Biochim Biophys Acta* 2009;1791:942-8.
39. Kim S, Lee J, Lee SK, Bae SY, Kim J, Kim M, et al. Protein kinase C- α downregulates estrogen receptor- α by suppressing c-Jun phosphorylation in estrogen receptor-positive breast cancer cells. *Oncol Rep* 2014;31:1423-8.
40. Hong EJ, Levasseur MP, Dufour CR, Perry MC, Giguere V. Loss of estrogen-related receptor α promotes hepatocarcinogenesis development via metabolic and inflammatory disturbances. *Proc Natl Acad Sci U S A* 2013;110:17975-80.
41. Liu Y, Ye X, Zhang JB, Ouyang H, Shen Z, Wu Y, et al. PROX1 promotes hepatocellular carcinoma proliferation and sorafenib resistance by enhancing beta-catenin expression and nuclear translocation. *Oncogene* 2015;34:5524-35.
42. Zheng Y, Chen Z, Han Y, Han L, Zou X, Zhou B, et al. Immune suppressive landscape in the human esophageal squamous cell carcinoma microenvironment. *Nat Commun* 2020;11:6268.

ABSTRACT(IN KOREAN)

간암에서 DGAT2가 미토콘드리아 기능 이상에 미치는 역할

<지도교수 황성순>

연세대학교 대학원 의학과

이 요 섭

비알코올성 지방간의 유병률이 증가함에 따라 간암 환자들의 병인으로써의 지방간의 영향이 점차 대두되고 있다. 그러나 실질적으로 지방 대사가 지방간과 간암에서 어떻게 변화하는지 잘 알려지지 않았다. 본 논문은 지방간 환자와 간암 환자의 유전체 분석을 기반으로 지방 대사에 관여하는 유전자들이 지방간에서는 증가하는 반면 간암에서 특이적으로 감소하는 결과 확인하였다. 이 중 중성지방 합성 효소인 DGAT2가 간암에서 어떠한 역할을 가졌는지 확인하고자 간암 세포주인 HepG2에서 DGAT2 유전자를 억제하여 그 기능이 손실되었을 때 변하는 요인 관찰하였으며, 간암 환자들이 가지고 있는 요인들과 비교하였을 때 어떠한 공통점을 가졌는지를 보았다. DGAT2의 기능이 감소하였을 때 세포주에서 지방 축적의 감소와 함께 세포의 성장률이 증가하는 것을 확인하였다. 흥미로운 점은 세포 내 미토콘드리아의 크기와 기능에서 확인한 감소를 관측하였다. 특히 이러한 미토콘드리아의 영향은 기존 간암 환자들에서도 확인할 수 있었으며 이러한 기능 감소는 환자의 예후에 악영향을 미치는 것으로 확인되었다. 이러한 대사적 변화의 원인을 찾기 위해 유전체 정보를 기반으로 전사인자들의 활성도를 분석하였고 ESRRA라는 전사인자의 활성 저하로 인해 미토콘드리아의 기능이 감소한다고 판단하였다. 특히 핵 안의 단백질을 확인해본 결과 실질적인 ESRRA의 양이 감소하였으며, 해당 전사인자의 저해제로 알려진 PROX1의 결합이 증가한 것을 확인할 수 있었다. 이러한 데이터를 기반으로 DGAT2는 ESRRA-PROX1 전사인자의 결합을 유도하여 미토콘드리아 기능 저해를 일으킨다는 것을 확인할 수 있었다.

핵심되는 말: 간암, 지방대사, 미토콘드리아, DGAT2, ESRRA, PROX1